Journal for ImmunoTherapy of Cancer

BND-22, a first-in-class humanized ILT2-blocking antibody, promotes antitumor immunity and tumor regression

Ilana Mandel ,[1] Dana Haves Ziv,[1] Ilana Goldshtein,[1] Tsuri Peretz,[1] Dror Alishekevitz,[1] Anna Fridman Dror,[1] Motti Hakim,[1] Sharon Hashmueli,[1] Itay Friedman,[1] Yair Sapir,[1] Rita Greco,[2] Hongjing Qu,[2] Frank Nestle,[2] Dmitri Wiederschain,[2] Lily Pao,[2] Sharad Sharma ,[2] Tehila Ben Moshe[1]

To cite: Mandel I, Haves Ziv D, Goldshtein I, *et al*. BND-22, a first-in-class humanized ILT2-blocking antibody, promotes antitumor immunity and tumor regression. *Journal for ImmunoTherapy of Cancer* 2022;**10**:e004859. doi:10.1136/jitc-2022-004859

► Additional supplemental material is published online only. To view, please visit the journal online (http://dx.doi.org/10.1136/jitc-2022-004859).

SS and TBM are joint senior authors.

Accepted 17 July 2022

[1]Biond Biologics, Misgav, Israel
[2]Oncology Reseach, Sanofi, Cambridge, Massachusetts, USA

Correspondence to
Dr Ilana Mandel;
ilana@biondbio.com

Dr Sharad Sharma, Oncology Research, Sanofi, Cambridge, MA, USA;
sharad.sharma@sanofi.com

ABSTRACT

Background Cancer immunotherapy has revolutionized cancer treatment. However, considering the limited success of immunotherapy to only some cancer types and patient cohorts, there is an unmet need for developing new treatments that will result in higher response rates in patients with cancer. Immunoglobulin-like transcript 2 (ILT2), a LILRB family member, is an inhibitory receptor expressed on a variety of immune cells including T cells, natural killer (NK) cells and different myeloid cells. In the tumor microenvironment, binding of class I MHC (in particular HLA-G) to ILT2 on immune cells mediates a strong inhibitory effect, which manifests in inhibition of antitumor cytotoxicity of T and NK cells, and prevention of phagocytosis of the tumor cells by macrophages.

Methods We describe here the development and characteristics of BND-22, a novel, humanized monoclonal antibody that selectively binds to ILT2 and blocks its interaction with classical MHC I and HLA-G. BND-22 was evaluated for its binding and blocking characteristics as well as its ability to increase the antitumor activity of macrophages, T cells and NK cells in various in vitro, ex vivo and in vivo systems.

Results Collectively, our data suggest that BND-22 enhances activity of both innate and adaptive immune cells, thus generating robust and comprehensive antitumor immunity. In humanized mice models, blocking ILT2 with BND-22 decreased the growth of human tumors, hindered metastatic spread to the lungs, and prolonged survival of the tumor-bearing mice. In addition, BND-22 improved the antitumor immune response of approved therapies such as anti-PD-1 or anti-EGFR antibodies.

Conclusions BND-22 is a first-in-human ILT2 blocking antibody which has demonstrated efficient antitumor activity in various preclinical models as well as a favorable safety profile. Clinical evaluation of BND-22 as a monotherapy or in combination with other therapeutics is under way in patients with cancer.

Trial registration number NCT04717375.

WHAT IS ALREADY KNOWN ON THIS TOPIC

⇒ While cancer immunotherapy has revolutionized cancer treatment, there is a constant need for developing new treatments that will result in higher response rates in patients with cancer.

WHAT THIS STUDY ADDS

⇒ The study described herein presents evidence for the role of immunoglobulin-like transcript 2 (ILT2) as a 'multi-immune cell checkpoint' which serves as an important immune evasion mechanism for tumors. In addition, the design and pharmacological activity of a novel, first-in-class, humanized ILT2 blocking monoclonal antibody, BND-22, is described.

HOW THIS STUDY MIGHT AFFECT RESEARCH, PRACTICE AND/OR POLICY

⇒ The results show that the inhibition of the ILT2 axis holds a great promise as monotherapy and in combination with established cancer therapies.

BACKGROUND

Cancer immunotherapies, which target tumor immune evasion mechanisms, have transformed clinical cancer care.[1] Immune checkpoint inhibitors, such as antibodies against programmed cell death protein-1 (PD-1), programmed death-ligand 1 (PD-L1) and cytotoxic T-lymphocyte-associated protein-4 are now approved for the treatment of multiple cancer types. Despite this, only a small percentage of patients with cancer benefit from checkpoint-inhibitor therapies. In addition, late relapses are emerging with longer follow-up, suggesting the emergence of acquired resistance.[2] Such resistance develops due to either the inability of T cells to infiltrate into tumors or to tumor-derived suppressive mechanisms overcoming antitumor functions of T cells. Most current immunotherapy regimens target T cells, yet myeloid cells, which constitute a larger cellular milieu of the tumor microenvironment, also play an important role in controlling overall tumor immunity.[3] Therefore, immunotherapies that can promote functions of both T cells (adaptive immunity) and macrophages (innate immunity) may generate a more robust

antitumor response, thus overcoming the limitations of current checkpoint inhibitors.[4]

Ig-like transcripts (ILTs) are a family of immune-modulating receptors expressed on various immune cells.[5] Immunoglobulin-like transcript 2 (ILT2) (leukocyte Ig-like receptor 1/CD85j/LILRB1), a member of the ILT family, is an inhibitory receptor expressed on both adaptive and innate immune cells including T cells, natural killer (NK) cells and various myeloid cells.[6–10] In T cells, ILT2 is highly expressed in a distinct CD8 T-cell population called effector memory T cells re-expressing CD45RA (T_{EMRA} cells).[11 12] ILT2 binds to the classical (HLA-A and -B) and non-classical (HLA-G, HLA-E, and HLA-F) major histocompatibility complex (MHC) class I molecules; however, its binding affinity to HLA-G is threefold to fourfold higher than to classical MHC I molecules.[10] Besides its physiological role in maternal–fetal tolerance, HLA-G is commonly expressed by solid tumors and has been associated with worse prognosis in multiple cancers including colorectal, esophageal, gastric, liver, lung, and cervical cancers.[13–16]

The interaction of ILT2 with its ligands in the context of an immune reaction can lead to impairment of immune cell proliferation, differentiation, cytotoxicity, cytokine secretion, and chemotaxis; and induction of regulatory T cells and myeloid-derived suppressor cells (MDSC) or M2-type macrophages,[16–20] thus allowing tumor cell evasion. ILT2 has been shown to inhibit multiple T-cell functions critical for antitumor immunity including cytokine production, cytotoxicity, and proliferation.[11 21–25] ILT2 inhibits NK-cell cytotoxicity and their ability to secret proinflammatory cytokines,[7 21 26–28] which can be restored by blocking ILT2.[7] In addition, it has been recently demonstrated that interaction of ILT2-expressing macrophages with class I MHC expressing tumor cells can convey a 'do not eat me' signal, which prevents the phagocytosis of tumor cells by macrophages.[18] These collective observations identify the ILT2-mediated signaling axis as a potential novel target for anticancer immunotherapy.

Here we present evidence for the role of ILT2 as a novel immune checkpoint, which serves as an important immune evasion mechanism for tumors. Furthermore, we describe the design, pharmacological activity, and non-clinical safety assessment of a novel, first-in-class, humanized ILT2 blocking monoclonal antibody. Collectively, the results provide the foundation for clinical testing of BND-22 in patients with solid tumors as monotherapy or in combination with PD-1 or tumor targeting therapeutics.

MATERIALS AND METHODS

Cells

Cell media and supplements were obtained from Biological Industries. Cell lines used in this study include A375 (ATCC, CRL-1619), A253 (ATCC, HTB-41), BW 5147.3 (BW; ATCC, TIB-47), 721.221 (ATCC, CRL-1855), 786-O (ATCC, CRL-1932), Jurkat (ATCC, TIB-152), COLO-320 (ATCC, CCL-220.1), and MEL526.

A253 and A375 were transfected to stably express human HLA-G1 using jetPEI (Polyplus). BW cells were transfected to express the extracellular part of human ILT2 or ILT4 and the intracellular part of mouse zeta chain using the Amaxa Nucleofector (Lonza) and Ingenio Kit (Mirus). 721.221 cells were transfected to express human HLA-G1, BW cells to express cynomolgus ILT2, COLO-320 to express human HLA-G1 and Jurkat cells to express human ILT2 using the Amaxa Nucleofector and V Kit (Lonza). G418 (Sigman-Aldrich) was used for selection and generation of stable clones. A375 WT cells or A375-HLA-G cells were also transfected to express OKT3scFv-CD14[29] followed by selection with hygromycin (Sigman-Aldrich). Primary cells used in this study include tumor-infiltrating lymphocytes (TILs) expanded from a melanoma patient (purchased from Sheba Medical Center).

Generation of single-cell suspensions from tumor samples

Tumor samples were obtained from biobanks of Rambam Medical Center and the Galilee Medical Center. Samples were digested into single-cell suspensions using DNase 1 type IV (30 U/mL), hyaluronidase type V (100 µg/mL) and collagenase (1 mg/mL). The samples were digested for 2 hours at 37°C followed by filtration through a cell strainer (70 µm) and washing in PBS to generate a single-cell suspension.

Isolation of peripheral blood mononuclear cells (PBMC)

Buffy coat samples were obtained from blood bank of healthy donors and patients with cancer following informed consent. Samples were diluted 1:2 in PBS and PBMCs were isolated using LSM gradient (MP Biomedicals) by centrifuging (1000×*g*, for 15 min) at room temperature without brakes. PBMCs were harvested, treated with red blood cell lysis buffer (Biological Industries), washed twice with PBS and used fresh or kept frozen in liquid nitrogen. The characteristics of the patients with cancer included in the study are detailed in the following table. The healthy donor samples acquired from the blood bank (n=6) were anonymous.

	Patients (N=23)
Gender n (%)	
Male	18 (78)
Female	5 (12)
Age (years)	
Median	62±12.3
Cancer type, n (%)	
Kidney cancer (renal cell carcinoma)	6 (26)
H&N cancer (HNSCC)	7 (20)
Esophagus cancer	4 (17)
Colon cancer	4 (17)
Lung cancer (non–small cell lung cancer)	2 (9)

Immunohistochemistry (IHC) of HLA-G

Tissue microarrays from different cancer types (Biomax) were subjected to antigen retrieval in citric buffer followed by staining with HLA-G antibodies (Sigma Aldrich, SAB2702386) and detection with ZytoChem Plus HRP-Polymer Anti-Rabbit (Zytomed, ZUC032-100) and DAB (3,3′-Diaminobenzidine) staining. Sections were then lightly counterstained with hematoxylin, dehydrated through ascending ethanols and mounted in DPX. IHC score was calculated by staining intensity multiplied by percentage of positive cells (Smart Assays). The following arrays were used in the study: ES809 (n=80, median age 59±8, male:female ratio (M:F) 75%:25%); HN802b (n=67, median age 55±12.2, M:F 87%:13%); ST1001a (n=57, median age 58.0±10.0, M:F 82%:18%) and CO20813a (n=143, median age 60±12.6, M:F 55%:45%). Healthy tissues constituted of the normal samples included in ES809 and HN802b (n=14, median age 34±13.1, M:F 57%:43%).

Soluble HLA-G ELISA

Levels of soluble HLA-G were detected in plasma samples from patients with cancer and healthy controls (DX biosamples) using a commercial ELISA according to the manufacturer's instructions (AVIVA, HKEH00979) (n=20 for each cancer type; characteristics are stated as follows).

M:F (%:%)	Age (median+SD)	Sample type
50:50	44±6.6	Healthy donors
45:55	61±11.4	Colorectal cancer
69:31	58±10.2	Head and neck cancer
65:35	60±8.0	Gastric cancer
0:100	58+12.5	Ovarian cancer
40:60	62±9.1	Pancreatic cancer
55:45	61±8.3	Kidney cancer (renal cell carcinoma)
85:15	65±10.6	Lung cancer (non–small cell lung cancer)
85:15	66±11.3	Bladder cancer
0:100	66±13.3	Breast cancer

Epitope mapping of BND-22

Initial in silico epitope mapping was performed by MAbSilico. The structure of ILT2 used was modeled using the structures 6AEE (four Ig-like domains, some loops missing), 1VDG (unpublished, domains 1 and 2), 1G0X (domains 1 and 2), and 4LL9 (domains 3 and 4).[30 31] A three-dimensional model of the antibody was built using Modeler. Empirical mapping was performed by Neoproteomics using hydroxyl radical footprinting (HRF) and mass spectrometry techniques.

Xenograft mice tumor models

For the melanoma lung lesions model, 5–12 SCID-NOD mice/group were engrafted IV with MEL526-HLA-G cells (4×10^6). PBMCs (15×10^6) from different healthy donors were injected intravenously into the mice on days 2, 10 and 18 or on days 15, 25, 35 and 51. Interleukin (IL)-2 (75×103 U/ mouse; Proleukin Novartis Pharma) was administered intraperitoneally every other day. A blocking ILT2 antibody (maILT2, hybridoma derived 19E3), BND-22, anti-PD1 (nivolumab, BMS), or a control IgG (BioXcell, BE0019-1 or Sino, HG4K) was administered at 10 mg/kg two times a week according to the treatment groups. Mice were monitored for weight and well-being by a person blinded to the experimental procedure. At the endpoint, full-body evaluation of metastasis was conducted; the lungs were photographed, harvested and weighed in order to record tumor burden.

For the subcutaneous (SC) colon cancer macrophage model, 1×10^6 COLO-320-HLA-G were injected subcutaneously to the right flank of 9 SCID NOD mice/group together with human macrophages which were generated from monocytes isolated from the blood of healthy donors (2×10^6). The mice were administered BND-22 or a control IgG4 (BioLegend, 403702), 20 mg/kg each. The antibodies were given SC on tumor inoculation day and four additional injections intravenously at days 3, 7, 10 and 14. Mice were monitored three times a week for weight, survival and for tumor volume using caliper measurement by a person blinded to the experimental procedure. Tumor volume was calculated as (small diameter^2×large diameter)/2.

For the humanized head and neck (H&N) cancer model, humanized NSG mice (Jackson, #705557/NSG; 17–19 weeks) were engrafted with CD34+ immune cells from three different human donors (12 mice/group). After 14 weeks, the mice were examined for the presence of immune cells by flow cytometry (FACS) analysis. Only mice with at least 25% human CD45+ cells in their peripheral blood were included in the study. The mice received subcutaneous injections of 1×10^6 A253-HLA-G mixed with an equal volume of Matrigel. Once the tumors were established (average of 80 mm^3), the mice were randomly divided into two groups that were administered intravenously with BND-22 or control hIgG4 (Sino, HG4K) at 10 mg/kg two times a week. Mice were monitored two times a week for signs of morbidity and tumor volumes were measured.

Tumor growth inhibition (TGI) was calculated by the following formula: 100−(group average tumor weight/control average tumor weight)×100.

Statistical analysis

Data are presented as means±SEM as stated in the figure legends. Statistically significant differences were tested using specific tests as indicated in the figure legends. A p value of <0.05 was considered statistically significant. Quantitative and statistical analyses of the data were preformed using Graphpad Prism V.8.1 software. EC_{50} values were determined using non-linear regression curve, fit variable slope (four parameters). In in vivo

experiments, outliers were removed from different evaluations according to Grubb's test.

RESULTS

ILT2 and HLA-G are highly expressed in the tumor microenviorment (TME) and peripheral blood of patients with cancer

The expression of ILT2 was first evaluated in peripheral blood samples from patients with cancer. Interestingly, it was found that the percentages of CD4 T cells, CD8 T cells, and NK cells that express ILT2 are significantly higher in the periphery of patients with cancer in comparison to healthy controls (figure 1A). These results suggest that ILT2 upregulation can serve as a mechanism for immune evasion in several tumor indications. To understand which immune cell populations express ILT2 in the tumor microenvironment, fresh tumor samples from patients with cancer were evaluated by flow cytometry. Overall,

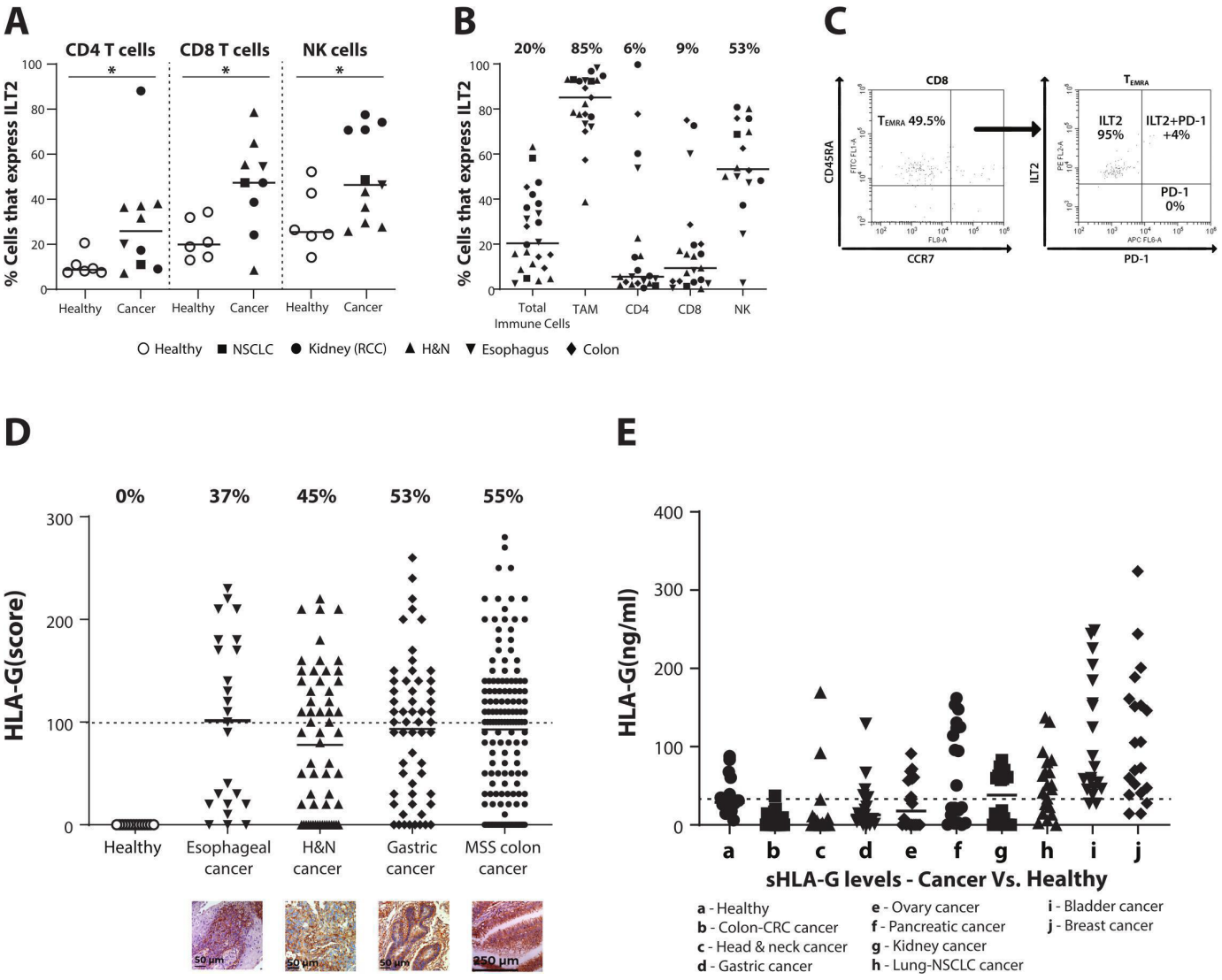

Figure 1 ILT2 and HLA-G are highly expressed in the TME and the periphery of patients with cancer. (A) PBMCs were isolated from the blood of the indicated patients with cancer or from healthy donors. The percentage of ILT2-expressing NK cells, CD8 and CD4 T cells was evaluated by flow cytometry. *P<0.05; Unpaired Student's t-test. (B) Single-cell suspensions were prepared by enzymatic digestion of fresh tumors isolated surgically from patients with various cancer indications. The percentage of ILT2 expression in total intratumoral immune cells, TAMs, CD8, CD4 T cells and NK cells was evaluated by flow cytometry as mentioned in the online supplemental material. The median percentage of ILT2-positive cells for each immune cell population is indicated. (C) Dot plots representative from evaluation of the levels of CD8 T_{EMRA} cells (left) and ILT2 and PD-1 expression in intratumoral CD8 T_{EMRA} cells (right) from an esophageal cancer patient. (D) Tissue microarrays from the indicated cancer types were stained with anti-HLA-G antibody for IHC. The percentages in the graph indicate patients with cancer samples that had a higher staining score (above 100). (E) Soluble HLA-G protein was evaluated in plasma samples collected from patients with cancer (n=20, each group) by ELISA. *P<0.05. H&N, head and neck; IHC, immunohistochemistry; ILT2, immunoglobulin-like transcript 2; MSS, microsatellite stable; NK, natural killer; NSCLC, non–small cell lung cancer; PD-1, programmed cell death protein-1; RCC, renal cell carcinoma; TAM, tumor-associated macrophage. T_{EMRA} cells, effector memory T cells re-expressing CD45RA.

ILT2 was found to be expressed in about 20% of the total immune cell population (CD45+) present in the TME of various patients with cancer. A high percent of macrophages and NK cells expressed ILT2 in TME (85%±3.2% and 53%±6.5%, respectively) (figure 1B). Lower frequencies of ILT2-expressing cells were observed in CD4 and CD8 T cells. However, within T cells, highly differentiated CD8 T_{EMRA} cells (CD45RA+CCR7−) selectively exhibited ILT2 expression. Interestingly, a low frequency of PD-1 expression was detected in this CD8 T-cell population, whereas PD-1 expression was mostly confined to 'non-T_{EMRA}' CD8 T-cell population (figure 1C).

Similarly, when performing a gene set enrichment analysis bioinformatic analysis of the The Cancer Genome Atlas (TCGA) database using The Cancer Immunome Atlas (www.tcia.at), a correlation was observed between higher ILT2 expression and enrichment of MDSC and 'M2-type' macrophages in patients with cancer (online supplementary figure S1A,B). In addition, when examining enrichment of CD8 T_{EMRA} cells across various tumor indications using the TCGA database, 22.8%–47.3% of patients had high levels of T_{EMRA} cells (online supplementary figure S1C). Furthermore, 57%–94% of the patients with high T_{EMRA} cells also showed high levels of ILT2 expression, indicating a strong association between ILT2 and T_{EMRA} cells (online supplementary figure S1D). Collectively, these results demonstrate that in the TME, ILT2 expression is increased and mainly expressed by myeloid cells, NK cells and CD8 T_{EMRA} cells.

Expression of HLA-G, a high-affinity ligand of ILT2, was also evaluated in patients with cancer by IHC. An IHC score was calculated based on staining intensity and number of stained cells, and a score of >100 was considered as representative of high expression of HLA-G. Using this criterion, high expression levels of HLA-G were observed in 55% of patients with microsatellite stable colon cancer, 45% of squamous cell carcinoma of the patients with H&N cancer, 37% of patients with esophageal cancer and 53% of patients with gastric cancer (figure 1D). Furthermore, higher levels of soluble HLA-G were detected in the plasma of various patients with cancer in comparison to healthy controls (figure 1E). Taken together, these results demonstrate that upregulation of ILT2 and HLA-G is a common mechanism of immune suppression within the TME and periphery of patients among many types of cancers.

BND-22 binds ILT2 with high affinity and selectivity

BND-22, a novel humanized immunoglobulin G4 (IgG4) monoclonal antibody with antagonist characteristics against human ILT2, was generated using hybridoma technology. Evaluation of the binding kinetics of BND-22 to human ILT2 using SPR BIAcore technology showed that BND-22 has strong and stable binding to ILT2 with an equilibrium dissociation constant (kd/ka) ranging from 1.26 nM to 4.48 nM (figure 2A). A similar dose-dependent binding to ILT2 expressed by a transfected cell line (BW-ILT2) was observed by flow cytometry (EC_{50}=0.05 µg/mL, figure 2B). BND-22 is selective to ILT2 and did not bind to other ILT family members that are highly homologous to ILT2 (eg, ILT4, ILT6, and LILRA1) (online supplementary figure S2).

BND-22 blocks binding of ILT2 to class I MHC molecules by inhibiting interactions in the B2M-binding region

When examining the binding of recombinant ILT2 to HLA-G-expressing A375 cells in the presence of varying doses of BND-22, BND-22 prevented the binding of ILT2 to HLA-G in a dose-dependent manner (IC_{50}=0.314 µg/mL, figure 2C). In addition, the ability of BND-22 to functionally block the interaction between either HLA-G or HLA-A2, and ILT2 was further examined in a BW ILT2/mouse Z-chain chimera cell-based reporter assay. Using this assay, it was demonstrated that BND-22 can efficiently block the interaction of ILT2 with both classical (HLA-A2) (figure 2D) and non-classical (HLA-G) MHC class I molecules (IC_{50}=0.179 µg/mL, figure 2E).

In silico epitope mapping revealed that BND-22 interacts with ILT2 at four epitope regions of ILT2 that are all found in the hinge section between domain 1 (D1) and domain 2 (D2). Interestingly, these epitopes have been identified as the interaction domains of ILT2 that specifically bind to beta-2-microglobulin (B2M) on HLA-A or HLA-G[32] (figure 2F,G). In addition, empirical epitope mapping using HRF and mass spectrometry techniques confirmed these results and identified binding residues within the D1 D2 domains of ILT2 that are known to be involved in the interaction of ILT2 with B2M (online supplementary table S1,S2).

BND-22 enhances the phagocytosis of cancer cells by macrophages

The ability of BND-22 to enhance the phagocytosis of tumor cells by macrophages was examined in vitro and ex vivo using two different experimental systems. Using a real-time analysis system, a dose-dependent enhancement of phagocytosis of HLA-G-positive cancer cells (A375) was observed over time (figure 3A). This is apparent when looking through the course of 18.0 hours (figure 3A) and at 12.5 hours (figure 3B). It is also evident when looking at the accumulation of the red signal that represents phagocytosis, which is higher in the samples treated with BND-22 versus control IgG (figure 3C). It was found that BND-22 can enhance phagocytosis of tumor cells expressing HLA-G or classical MHC-I (figure 3C,D).

BND-22 was also found to enhance the phagocytosis of patient-derived tumor cells that were obtained from patients with renal cell carcinoma (RCC), H&N cancer, and esophagus cancer. The magnitude of increase in phagocytosis differed between patients and were up to 1.2-fold compared with the isotype antibody (online supplementary figure S3). Interestingly, the ability of BND-22 to increase phagocytosis was comparable to CD47 blockade, which is a predominant mechanism to augment tumor cell phagocytosis (figure 3E). Additionally, to a higher relevance to the clinical settings, BND-22

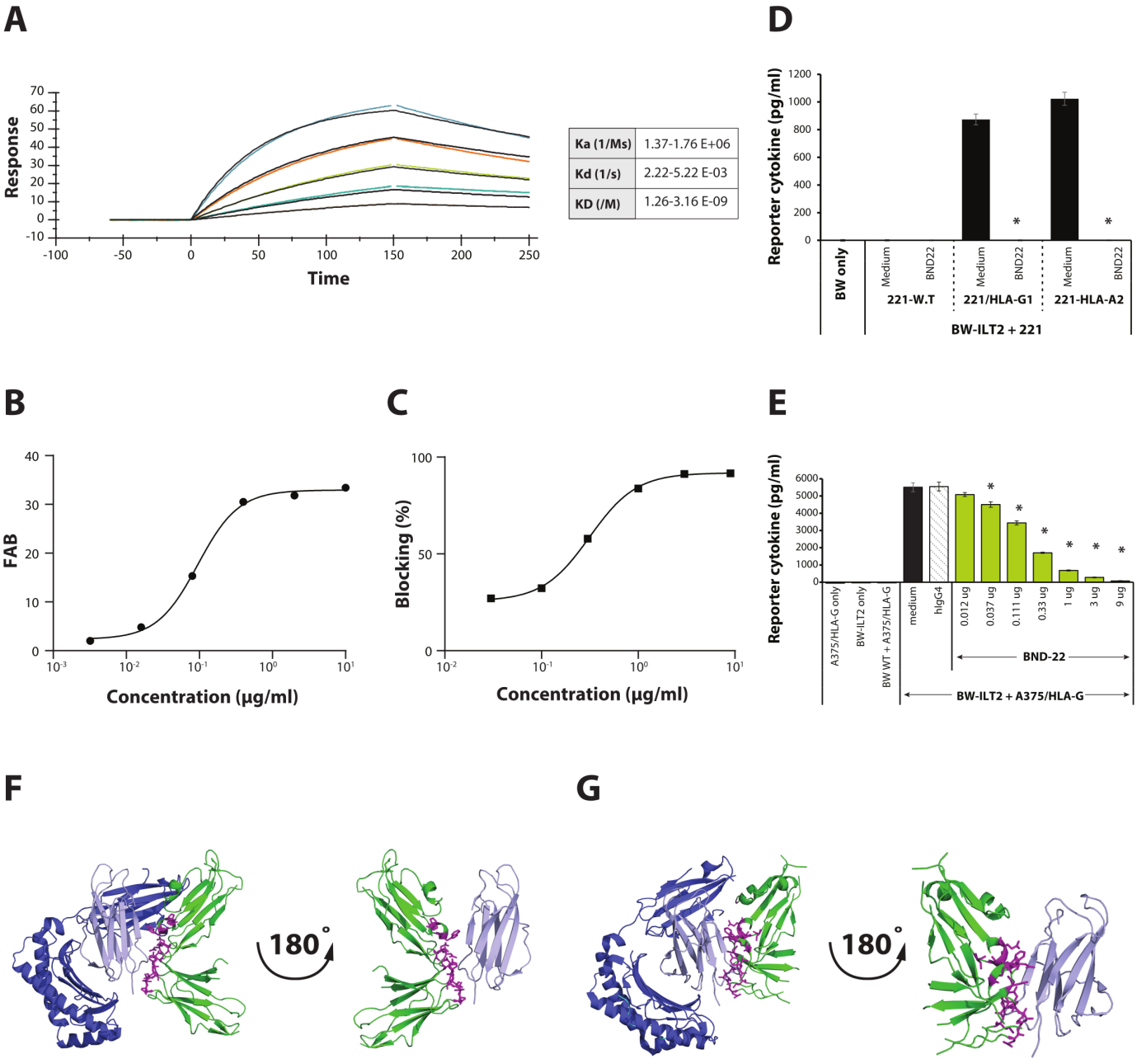

Figure 2 BND-22 selectively binds to ILT2 and blocks its interaction with HLA-G and HLA-A2 by blocking ILT2 binding to the B2M-binding region. (A) The binding of BND-22 to human ILT2 as determined by multicycle analysis using the Biacore T200. Sensograms and fitted curves (1:1 binding model) are displayed as well as the summary of the kinetic parameters. Recombinant human ILT2 in six points in the range of 25–0.78 nM in twofold dilutions, represented by the different colors in the sensogram, was added to the system. (B) The binding of BND-22 to BW cells transfected with ILT2 as evaluated by flow cytometry. (C) A375-HLA-G cells were incubated with biotinylated ILT2-FC in the presence of various concentrations of BND-22 followed by staining with streptavidin–PE and FACS analysis. A graphical representation of the percentage of blocking compared with cells without antibody is shown. BW WT cells or BW cells transfected with ILT2-zeta (BW-ILT2) were incubated with 721.221 wildtype cells (221 W.T), or 721.221 transfected to express (221-HLA-G) or HLA-A2 (221-HLA-A2) (D) or with A375-HLA-G cells (E) in in the presence of various concentrations of BND-22, control IgG or PBS for 48 hours. The secretion of a reporter mouse cytokine was measured by ELISA. *P<0.05, unpaired Student's t-test. Three-dimensional ribbon or surface diagrams of ILT2 showing the epitope of BND-22 (pink) and its interaction on ILT2[44] with B2M (lilac) in complex with (F) HLA-A or (G) HLA-G.[45] B2M, beta-2-microglobulin; BW ILT2, BW cells transfected with ILT2-zeta; BW WT, BW wild type; FAB, fold above (isotype control) background; ILT2, immunoglobulin-like transcript 2; Ka, association rate constant (1/Ms); Kd, dissociation rate constant (1/s); KD, equilibrium dissociation constant (kd/ka).

also enhanced the phagocytosis of tumor cells from RCC and H&N patients by respective autologous macrophages in a dose-dependent manner (figure 3F,G).

BND-22 enhances the activity of antitumor T cells

The ability of BND-22 to alleviate ILT2-mediated inhibition on T cells was examined in different cellular systems.

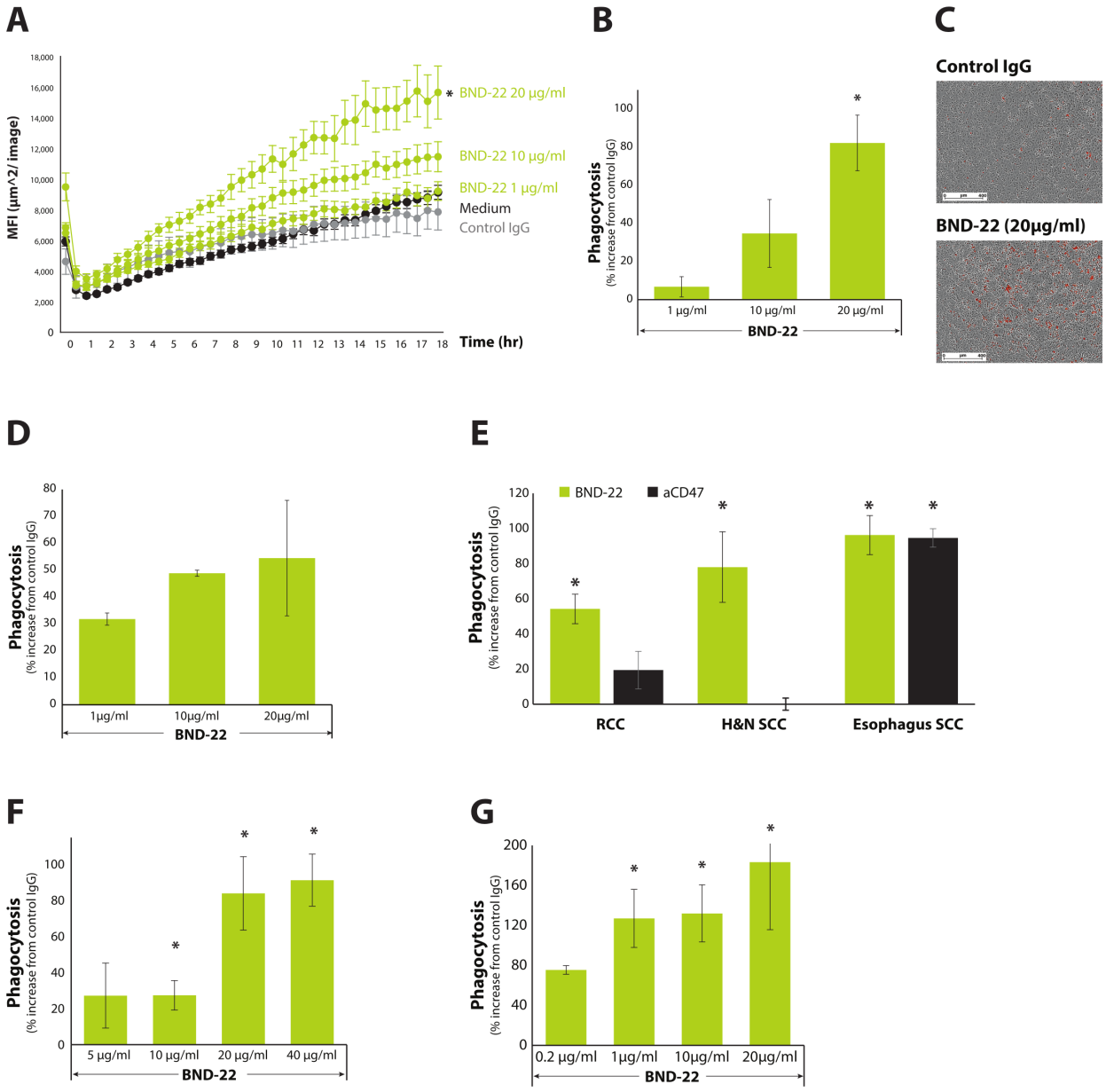

Figure 3 BND-22 enhances the phagocytosis of cancer cells by macrophages. A375-HLA-G cells were stained with pHrodo red cell labeling dye and added to monocyte-derived macrophages generated from healthy donors, along with the various indicated treatments in triplicates. (A) A representative kinetic quantification of phagocytosis is presented in a time-course of 18 hours as analyzed using Incucyte S3.(B) A single representative time point of the experiment at 12.5 hours is presented. Percent increase in macrophage-mediated phagocytosis with respect to control IgG (20 µg/mL) is presented. (C) Images of cells incubated in the presence of control IgG or BND-22 are presented. The red signals captured represent phagocytosis events. (D) Phagocytosis of A375 wild-type cells by macrophages. Single-cell suspensions were generated by enzymatic digestion of fresh tumors surgically isolated from patients with cancer (indicated in E,F), patients with RCC, and (G) patients with H&N cancer. The cells were stained with pHrodo red cell labeling dye and mixed with monocyte-derived macrophages generated from healthy donors or (E) from autologous patients (F,G), along with the various indicated treatment doses in triplicates. The percent increase in macrophage-mediated phagocytosis of tumor cells compared with control IgG is presented. MFI - mean fluorescence intensity. *P<0.05; unpaired Student's t-test compared with cells with control IgG. H&N, head and neck; RCC, renal cell carcinoma.

As depicted in figure 4, coculturing ILT2-expressing Jurkat T cells with A375 engineered to express OKT3 (anti-CD3) and HLA-G (figure 4A) or endogenous classical MHC-I (figure 4B) led to increased production of human IL-2 by BND-22 in a dose-dependent manner. Interestingly, on blocking HLA-G, with an HLA-G-specific antibody, the effect was much less significant than that of BND-22, suggesting that the ILT2 interaction with both classical and non-classical MHC-I plays a major role in suppressing T-cell function in this system (figure 4C). Using this system, it was also demonstrated that the increase in T-cell function by BND-22 is specific to its ability to block ILT2, as in ILT2-deficient wild-type Jurkat cells, BND-22 had no effect on IL-2 production.

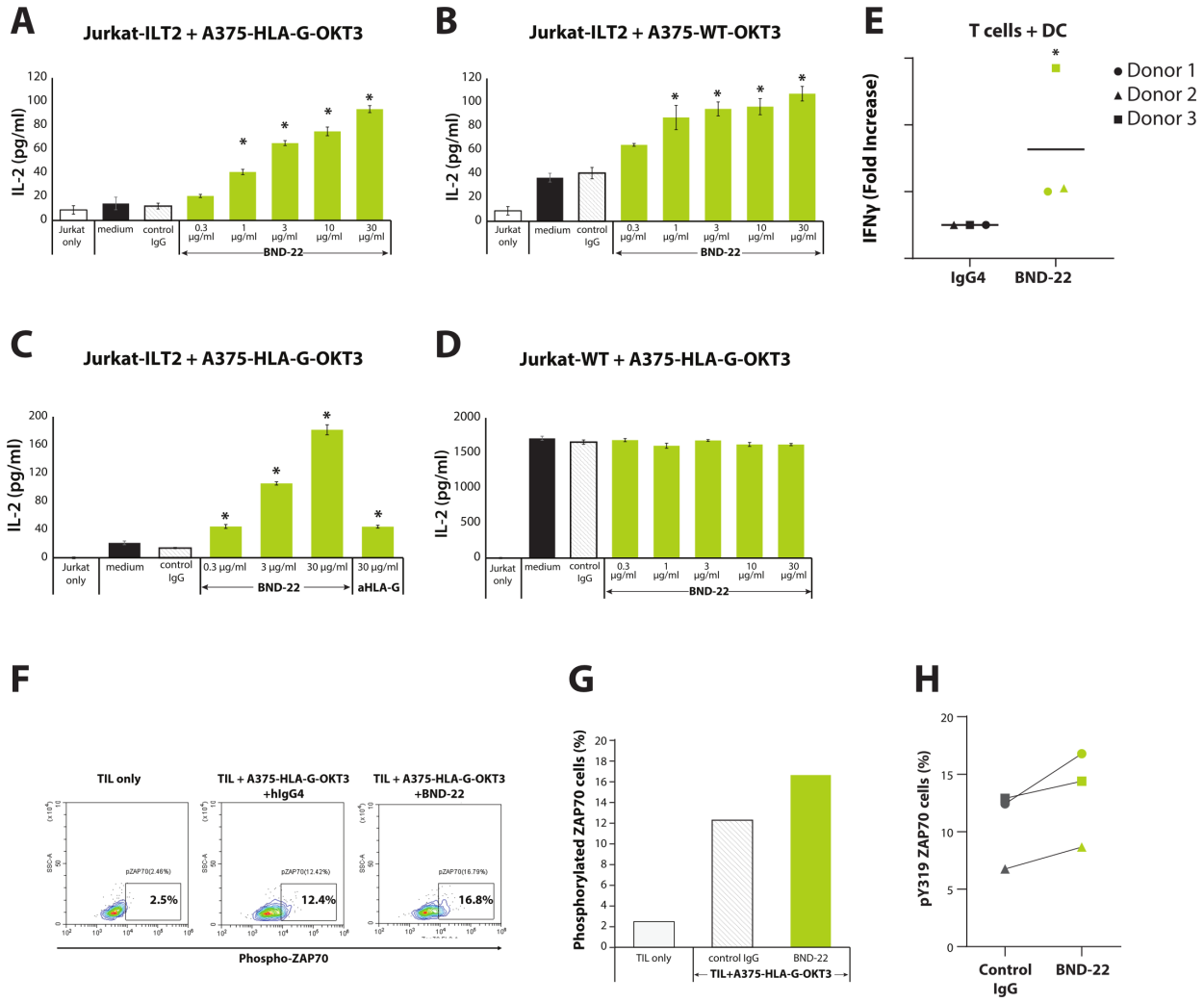

Figure 4 BND-22 enhances T-cell activity against cancer cells. Jurkat cells transfected with ILT2 (Jurkat-ILT2, A–C) or wild-type Jurkat cells (Jurkat-WT, D) were incubated with mitomycin-treated OKT3-expressing A375 cells that were either MHC class I positive (A375-WT-OKT3, B) or HLA-G positive (A,C,D) in the presence of BND-22 control IgG or a HLA-G-specific blocking antibody. The amount of secreted human IL-2 was evaluated by ELISA kits following 48 hours. *P<0.001, one-way analysis of variance[46] followed by Dunnett's multiple comparisons test compared with control IgG. (E) DCs generated from monocytes and CD8 T cells (T cells) were isolated from healthy human donors. The cells were combined in an E:T of 5:1 together with the indicated treatments followed by detection of IFN-γ secretion on day 5 Representative results are shown. The mean±SE of values from three repeats per treatment is displayed. TILs were coincubated with A375-HLA-G-OKT3 cells for 5 min and immediately placed in 2% Paraformaldehyde (PFA) on ice followed by detection of phosphorylated ZAP70/Syk by flow cytometry. (F) Representative FACS analysis of the levels of phosphorylated ZAP70 in the indicated conditions. The cells were gated on ILT2+CD8 T cells. (G) A graphical representation of the results shown in F. (H) A summary of three experiments performed in similar conditions. DC, dendritic cell; E:T, effector-to-target ratio; IFN-γ, interferon gamma; IL, interleukin; TIL, tumor-infiltrating lymphocyte.

Furthermore, the basal IL-2 secretion was notably higher when comparing wild-type Jurkat cells to that of ILT2-transfected Jurkat cells, further demonstrating the inhibitory effect of ILT2 (figure 4C,D). The ability of BND-22 to increase T-cell function was also demonstrated in a primary human T cell-based mixed lymphocyte reaction (MLR) assay. The addition of BND-22 to cultures of allogenic T cells and dendritic cells (DCs) from various donors significantly increased interferon gamma (IFN-γ) secretion from the T cells (figure 4E). Thus, in addition to the results observed in Jurkat cells, it was demonstrated using primary cells that ILT2 mediates inhibitory activity in T cells, which could be reversed by BND-22.

Finally, when adding A375-HLA-G-OKT3 cells to TILs expanded from a patient with melanoma, BND-22 blocked the inhibitory activity of ILT2, leading to an increase in the phosphorylation levels of ZAP70 (figure 4F–H). These results demonstrate that BND-22 can directly disrupt ILT2-mediated signaling events that occur on ligand binding, thus leading to increased phosphorylation of key signaling elements which are involved in downstream activation of T cells.

BND-22 enhances NK-cell activity against cancer cells

The ability of BND-22 to enhance the cytotoxic capacity of NK cells was tested in both an NK cell line and primary human NK cells. A dose-dependent increase in NK cell-mediated target cell killing was observed against HLA-G and MHC class I-expressing cancer cells in the presence of BND-22 (figure 5A–D). Additionally, a corresponding increase in IFN-γ and granzyme B levels was also observed in the presence of BND-22 (online supplementary figure S4). The ability of BND-22 to increase the activity of primary NK cells against cancer cells demonstrated that BND-22 increased both the levels of intracellular IFN-γ as well as membranal CD107a (figure 5E,F). These results indicate an enhancement in the activity and cytotoxicity of primary NK cells in response to BND-22 in the presence of target HLA-G+ cancer cells. Furthermore, a correlation between the percentage of ILT2-expressing NK cells (CD56+ILT2+) and the ability to increase both IFN-γ and CD107a levels was observed (figure 5G). In a separate set of experiments, on adding A253-HLA-G cells to NK cells, BND-22 increased the phosphorylation of Syk in comparison to control IgG (figure 5H–J), suggesting blockade of the NK inhibitory activity of ILT2. Collectively, these data show that ILT2-mediated signaling inhibits NK-cell function and can be reversed by ILT2 blockade by BND-22.

BND-22 enhances the antitumor activity of anti-PD-1 and tumor targeting antibodies

In order to evaluate the rationale to combine BND-22 with anti PD-1, the expression of PD-1 and ILT2 was examined on immune cells from patients with cancer. An analysis of an available database for T cells isolated from patients with colorectal cancer (CRC) (http://crctcell.cancer-pku.cn) revealed that ILT2 and PD-1 are expressed on different CD8 T-cell populations in tumors. ILT2 is expressed in the T_{EMRA} cell population, whereas PD-1 expression was confined to central memory T cells and exhausted T cells (T_{EX}) (figure 6A).[33] Similar results were observed in intratumoral T cells from a patient with esophageal cancer (figure 1C). The intratumoral T_{EMRA} cells in this patient were found to express ILT2 but not PD-1. Additionally, bioinformatic analysis of published data revealed that ILT2 expression was increased in 48% of melanoma patients after treatment with anti-PD-1 (Nivolumab) (figure 6B), which suggested that ILT2 upregulation is a potential mechanism for developing anti-PD1 resistance.

The effect of combining BND-22 with anti-PD-1 was first evaluated in an MLR assay. On testing for single agent activity, both BND-22 and anti PD-1 antibody enhanced IFN-γ secretion from T cells in the presence of allogeneic dendritic cells. Interestingly, IFN-γ production by T cells was further enhanced when a combination of both antibodies was tested (figure 6C). Similarly, co-culture of tumor cells with autologous PBMCs from a patient with colon cancer demonstrated that BND-22 and anti-PD-1 antibody can increase tumor necrosis factor alpha (TNFα) secretion. The combination of these two antibodies resulted in a significant synergistic effect (figure 6D).

Antibody Dependent Cellular Phagocytosis (ADCP) is one of the main mechanisms of anti-tumor activity for tumor-targeting antibodies (eg, cetuximab, rituximab).[34] Since ILT2 is highly expressed by macrophages and can suppress their phagocytic activity,[18] there is a rationale for combining BND-22 with ADCP-inducing antibodies. The ability of BND-22 to further enhance anti-EGFR antibody (cetuximab) mediated ADCP was evaluated against an EGFR expressing cell line. Using a real-time live-cell analysis system, it was observed that when tested as a single agent, both BND-22 and Cetuximab increased phagocytosis of the EGFR-expressing cancer cell lines. Interestingly, the combination of the antibodies enhanced the phagocytosis to a higher level than single agent activity (figure 6E,F).

Taken together, these results demonstrate the rational to combine BND-22 with either PD-1 blockers or tumor targeting therapies such as Cetuximab to further enahnce antitumor immune activity.

BND-22 increases the antitumor activity of lymphocytes and macrophages in vivo

ILT2 shares low homology with the mouse homolog of ITL2, PirB,[5] and BND-22 cannot bind PirB (data not shown). Therefore, several different xenograft models were used to study the mode of action of BND-22. The ability of BND-22 to elicit anti-tumor activity of lymphocytes and consequently prevent metastasis was evaluated in a human xenograft lung lesion model in NOD SCID mice with human PBMC engraftment. In this experiment, tumor burden and numerous lung lesions were developed in the lungs of untreated mice or mice that received human PBMCs with control IgG . In contrast, blockade of ILT2 resulted in significant TGI (figure 7A, TGI of 58%). ILT2 blockade in this model led to prevention of metastasis so that lungs weight and morphology appeared closer to healthy non-tumor bearing lungs (figure 7A).

A similar model was used to demonstrate therapeutic efficacy of BND-22 in pre-established tumors. Metastatic melanoma was established in the lungs of NOD SCID mice with human PBMC engraftment. TGI was observed in the groups treated with BND-22 alone and in combination with anti-PD-1 (figure 7B; TGI of 55% and 57% respectively compared with the IgG group). A statistical trend was observed for the group treated with BND-22 +anti-PD-1 in comparison to the isotype control group (one-way ANOVA followed by Dunnett's multiple comparisons; p=0.0586). In addition, BND-22 alone or in combination with PD-1 blockade upregulated various activation markers such as CD69 and CD107a on T/NK cells in the tumors (online supplementary figure S5A,B). Interestingly, mice that received PBMCs from donors with a higher expression/frequency of ILT2 on CD8 T and NK cells had a more substantial increase in CD69 and CD107a post BND-22 treatment. This correlation suggests that treatment with BND-22 played a direct role

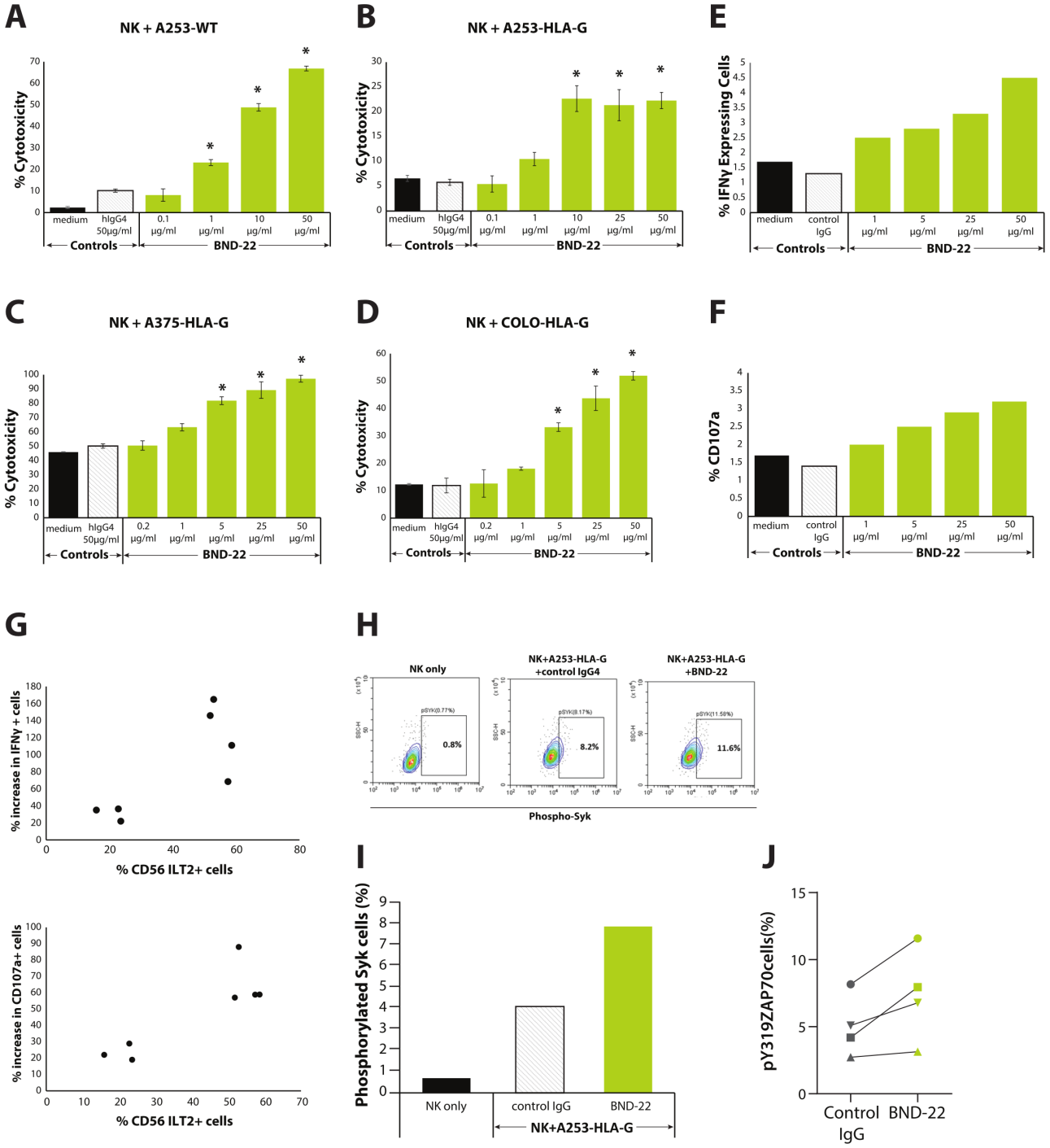

Figure 5 BND-22 enhances NK-cell activity against cancer cells. NK cells were incubated with the indicated concentrations of BND-22 or a control IgG; Target cells including A253-WT (A), A253-HLA-G (B), A375-HLA-G (C) and COLO 320-HLA-G (D) were added for an additional 5 hours at an E:T of 7.5:1. Representative results are shown. Results represent an average of % cytotoxicity±SE determined by LDH release assay in triplicates. WT cells express MHC-I; HLA-G transfected cells express both MHC-I and HLA-G. *p<0.02, One-way analysis of variance followed by Dunnett's multiple comparisons test compared with NK+target cells+control IgG. NK cells isolated from healthy donors were incubated with the indicated concentrations of BND-22 or a control IgG. A375-HLA-G cells were added for additional 5 hours at E:T of 8:1 followed by staining for intracellular IFN-γ, membranal CD107a, ILT2 and CD56 and analysis by flow cytometry. (E) The percentage of IFN-γ-positive NK cells in the CD56+ILT2+ population. (F) The percentage of CD107a-positive NK cells in the CD56+ILT2+ population. (G) Correlation between percentage of CD56+ILT2+ cells in the isolated NK cells and percent increase in IFN-γ (top) or CD107a (bottom) in the presence of A375-HLA-G and BND-22 (50 µg/mL) is presented for seven different donors tested. NK cell lines were cocultured with A253-HLA-G cells for a minute followed by immediately fixing in 4% PFA on ice and ZAP70/Syk phosphorylation was examined by flow cytometry. (H) Representative FACS plots showing phosphorylated SyK in the indicated conditions. (I) A graphical representation of the results shown in H. (J) A summary of four experiments performed in similar conditions. IFN-γ, interferon gamma; ILT2, NK, natural killer; WT, wild type.

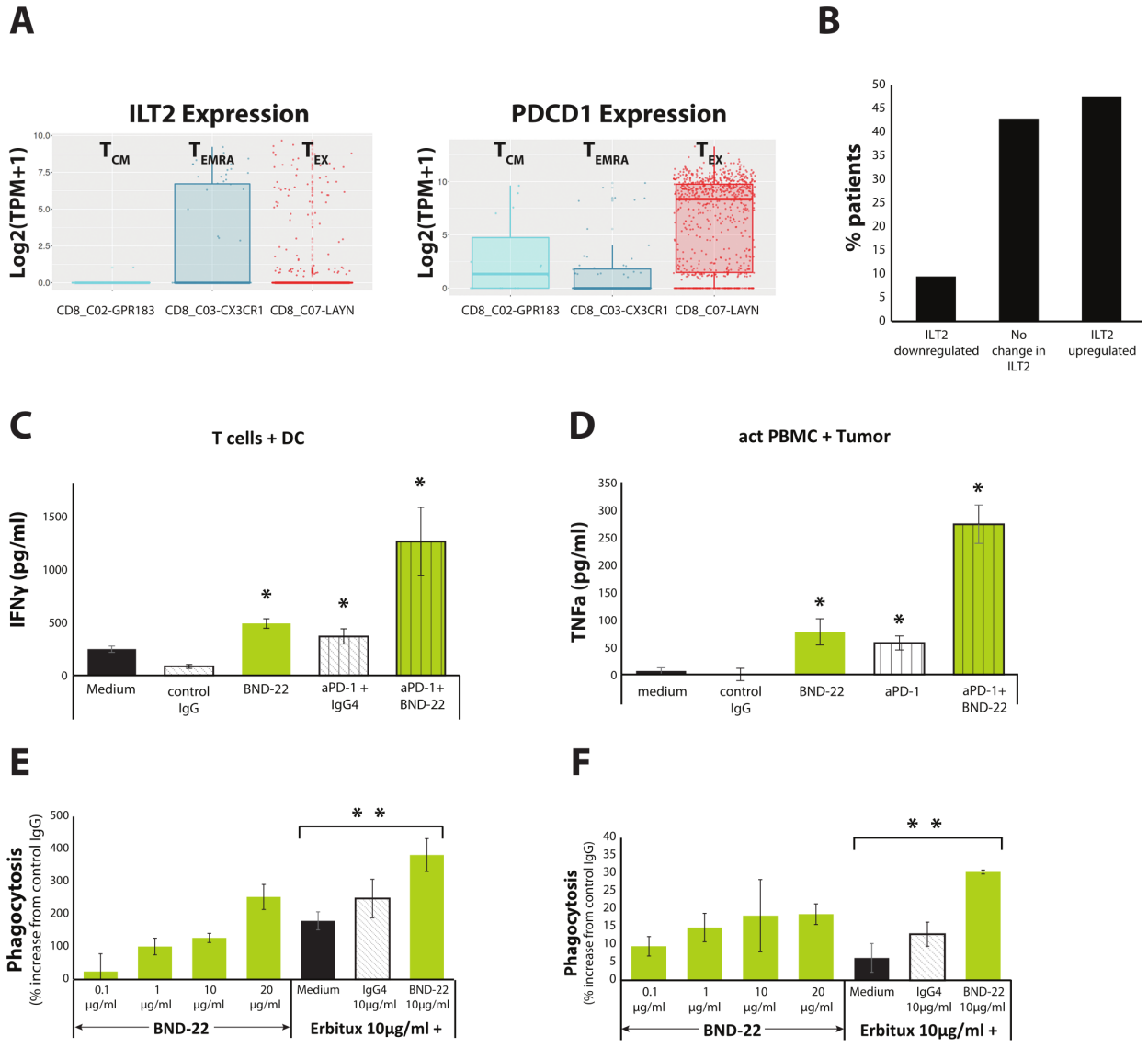

Figure 6 BND-22 enhances anti-tumor functions of anti-PD-1 or tumor targeting antibodies. (A) Analysis of ILT2 and PD-1 expression in intratumoral CD8 T cells from patients with CRC documented in http://crctcell.cancer-pku.cn/. (B) A bioinformatic analysis of ILT2 expression in melanoma patients treated with Nivolumab from.[47] The RNAseq data was used to calculate expression changes in patients with cancer post versus pre-Nivolumab treatment. Log2 ILT2 fold-change differences above 0.5 or below 0.5 were considered as increase and decrease in expression, respectively. (C) DCs were generated from monocytes and CD8 T cells were isolated from PBMCs of healthy human donors. The cells were combined in E:T of 5:1 ratio with the indicated treatments and IFN-γ was measured in culture supernatants at day 5. (D) Single-cell suspensions were prepared by enzymatic digestion of a fresh tumor isolated from a patient with colon cancer. PBMCs were isolated from the same patient and cocultured with the indicated treatments in presence of IL-2. TNFα secretion was detected by ELISA. Representative results are shown. The mean±SE of values from three repeats per treatment are displayed. Unpaired Student's t-test compared with control IgG for BND-22 or anti-PD-1, compared with anti-PD-1+IgG for anti-PD-1+BND-22.*P<0.05; (E) 786-O cells, or (F) A253-HLA-G cells were stained with pHrodo red cell labeling dye, washed and added to macrophages generated from monocytes isolated from healthy donors, along with the various treatments in triplicates. A single representative time point of the experiment at 9.5 hours is presented. The percentage of increase in phagocytosis compared with control IgG is presented. Unpaired Student's t-test compared with erbitux+medium. **P<0.01. CRC, colorectal cancer; DC, dendritic cell; IFN-γ, interferon gamma; ILT2, immunoglobulin-like transcript 2; PD-1, programmed cell death protein-1; T_{CM}, central memory T cells; T_{EMRA}, T cells re-expressing CD45RA; T_{EX}, exhausted T cells.

in intratumoral immune cell activation (online supplementary figure S5C,D). Taken together, these results support the mode of action of BND-22 as an enhancer of the cytotoxic activity of T and NK cells against cancer cells in vivo and shows that anti-ILT2 treatment can reduce tumor burden and eliminate metastasis.

The ability of BND-22 to enhance the anti-tumor activity of macrophages in vivo was evaluated in a subcutaneous humanized tumor mouse model. In this model, human macrophages, and human colon cancer cells (COLO-320-HLA-G) were transferred into SCID NOD mice. Administration of BND-22 resulted in 91% TGI in comparison

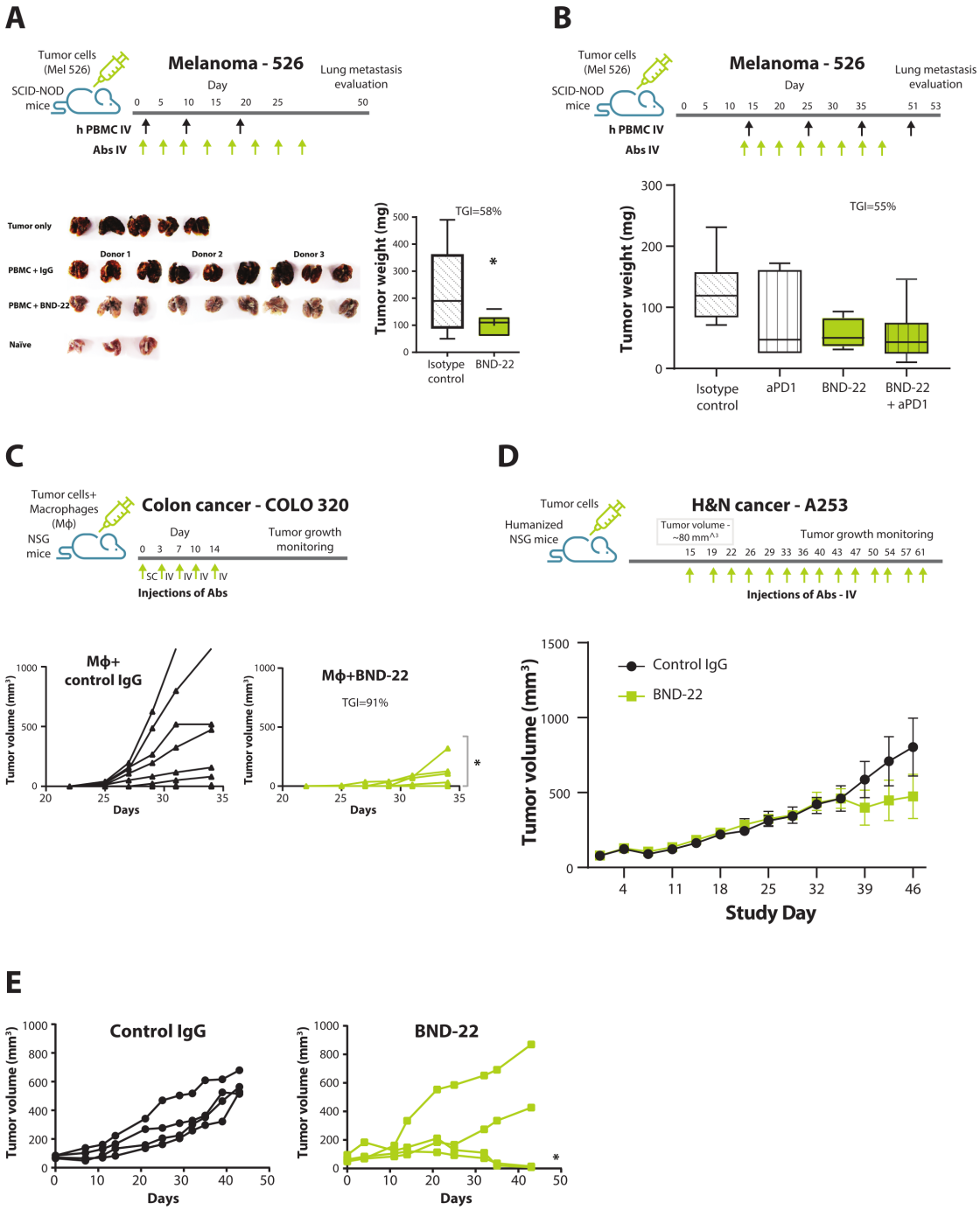

Figure 7 BND-22 inhibits tumor growth in vivo. (A,B) SCID-NOD mice were engrafted with MEL526-HLA-G cells intravenously. Human PBMCs isolated from healthy donors were transferred to the relevant groups together with IL-2 followed by antibody treatments (10 mg/kg each) starting from day 1 (A) or day 14 (B) according to the treatment schedules as indicated in the Materials And Methods section. At the endpoint, the mice were sacrificed; the lungs were weighted; and images were captured. Images showing the lung lesions developed by melanoma cells in the mice lungs from groups are presented (B). Tumor weight was calculated by subtracting naïve mouse lung weight from the lung weight of the experimental mouse. The median value from each group is presented in the graph as a vertical line (A,B). (C) NSG mice were engrafted SC with COLO-320 cells and human macrophages differentiated from monocytes isolated from healthy donors. The animals were treated with BND-22 or with control IgG (20 mg/kg) according to the treatment schedule outlined in the illustration. The data are presented as tumor growth curves from individual mice. Unpaired t-test was used to calculate statistical significance of TGI between the groups (A), One-way ANOVA followed by Dunnett's multiple comparisons was used (B). A two-way repeated measures ANOVA was used (C,E). Human CD34+cell-engrafted mice were inoculated with A253-HLA-G cells. The mice were treated at indicated treatment schedule with BND-22 or a control IgG (10 mg/kg) when tumors reached 80 mm3. (D) Mean of tumor growth in mice that received CD34+ cells from all three donors and were treated with either BND-22 or control IgG4. (E) Tumor growth in mice inoculated with CD34+ cells from one of the donors treated with either BND-22 or control IgG4. *P<0.05. ANOVA, analysis of variance; IL, interleukin; TGI, tumor growth inhibition.

to mice that received control IgG (p<0. 001 two-way repeated measures ANOVA) (figure 7C). Furthermore, BND-22 administration led to a prolonged/sustained TGI (online supplementary figure S6E). These results support the notion that in the absence of T/NK cells, BND-22 can enhance phagocytic activity of macrophages against tumor cells in vivo.

BND-22 generates a potent antitumor immune response and inhibits tumor growth in humanized tumor mouse models

In order to evaluate the ability of BND-22 to mediate anti-tumor activity in an in vivo model in which the entire human immune system is present, the efficacy of BND-22 was tested in a H&N cancer model (A253-HLA-G) in fully humanized NSG mice engrafted with human CD34+cord blood cells. Notably, these mice contain cells of both the lymphoid and myeloid compartments as evaluated in the periphery and tumors of the mice (online supplementary figure S5F and data not shown). In this model, administration of BND-22 caused 41% overall TGI (figure 7D). Interestingly, in mice receiving immune cells from one of the human donors, 50% of the mice showed complete tumor regression with BND-22 treatment (p<0.001 two-way repeated measures ANOVA, responding mice versus IgG-treated mice) (figure 7E). Furthermore, intratumoral increase in CD107a on CD8 T cells, M1/M2 ratio and CD80 expression on DCs confirmed that a potent anti-tumor immune response was elicited in the mice that responded to BND-22 treatment (online supplementary figure S5F) In addition, a correlation between ILT2 expression levels in the peripheral CD8 T cells of the mice and response to BND-22 was established (online supplementary figure S5G). These results demonstrate the ability of BND-22 to generate a robust, broad anti-tumor response by orchestrating an effect on both innate and adaptive immune cells thus leading to a shift in the environment of the tumor from suppressive to inflammatory.

DISCUSSION

LILRB family comprises of a number of regulatory, inhibitory receptors that are expressed on various immune cells. Recently, interesting data was generated in the clinic by inhibiting one of the LILRB members, LILRB2 (ILT4), in patients with cancer.[35] Therefore, inhibition of LILRB family members holds promise as monotherapy and in combination with established cancer therapies. Unlike ILT4, LILRB1 (ILT2) is widely expressed by immune cells T, NK, and myeloid cells, and negatively regulates both the innate and the adaptive immune system. Our clinical analysis suggests that ILT2 and HLA-G are further upregulated in the periphery and intratumorally in patients with cancer across many indications. Therefore, in context of tumor immunotherapy, ILT2 could be considered a 'multi-immune cell checkpoint' and its potential role in immune suppression in the TME provides a strong rationale for its targeting.[36]

Our in vitro, ex vivo and in vivo results demonstrate that ILT2 promotes both tumor growth and lung metastasis by compromising activation and functions of anti-tumor T cells, NK cells and macrophages. BND-22 is a first-in-class fully humanized ILT2 blocking antibody, which reverses immune suppressive functions of ILT2 and reduced tumor growth in mice by augmenting tumor specific immune responses. In our experiments, BND-22 enhanced the phagocytic activity of macrophages and the cytotoxic capability of both NK and T cells against tumor cells. Interestingly, BND-22 increased ZAP70/Syk signaling in both T and NK cells. Overall data presented in this report suggests that blocking ILT2 with BND-22 shifts the TME towards pro-inflammation.

BND-22 demonstrated clear anti-tumor activity in different in vivo models as evident by reduction in primary tumor growth and lung metastasis and increased survival in the BND-22 treatment groups. BND-22 was shown to mediate anti-tumor activity through a number of mechanisms including increasing the effector functions of T and NK cells. Additionally, BND-22 treatment caused an increase in the M1/M2 ratio within tumors and upregulation of costimulatory marker CD80 on DCs suggesting that blocking ILT2 increased the ratio of inflammatory compared with suppressive myeloid cells intratumorally. Although these tumor models can be valuable in demonstrating potency, the small number of mice in the humanized mice model and possibility of developing allogenic responses in the PBMC-engrafted lung lesion model need to be taken into consideration. Of note, the mice did not display any physiological symptoms that could point to graft-versus-host disease (GVHD) responses.

Blockade of PD-1/PDL-1 pathway is considered as the mainstay of cancer immunotherapy however, many patients receiving this therapy do not respond at all or experience relapses.[37] Therefore, there is an unmet need for additional complementary approaches, which can help improve overall response and survival in these patients. In this context, resistance to anti-PD-1/PD-L1 therapy could be mediated by additional immune checkpoint pathways. Recent findings have suggested that the ILT2/HLA-G pathway is upregulated in patients with cancer previously treated with anti-PD-1 drugs suggesting ILT2-mediated suppression as a potential resistance mechanism. It was demonstrated by us and others that PD-1 and ILT2 are expressed on different CD8 T cell subpopulations.[11 12] These studies demonstrated that PD-1 is primarily expressed by effector memory T cells and T_{EX}, whereas ILT2 expression is confined to T_{EMRA} cells in the TME. These observations suggest that due to lack of PD-1 expression, anti-PD-1 treatment is not effective in activating the T_{EMRA} cell population that could be present in large numbers in the TME. In addition, ILT2 expression and the number of T_{EMRA} cells that express ILT2 were shown to be increased following anti-PD-1 treatment.[38 39] Using computational biology, we observed that ILT2 expression was increased in 48% of melanoma patients that were previously treated with anti-PD-1. Considering that

increased levels of soluble HLA-G are also associated with reduced response to anti-PD-1 treatment,[40] we postulate that blocking of ILT2/HLA-G interactions with BND-22 will be effective to maximize the benefit of anti-PD1. Data presented in this manuscript also support this hypothesis. In addition, there is also a rationale to combine BND-22 with anti-EGFR antibody as demonstrated here. Patients expressing high levels of ILT2 were found to have an impaired ability to kill cancer cells in the presence of cetuximab and functional blockade with an ILT2 antagonist antibody restored Antibody-dependent cellular cytotoxicity (ADCC).[41 42] In addition, antibody-mediated ADCP (such as mediated by cetuximab) function can also be further enhanced by BND-22.[3443] In our studies, BND-22 enhanced tumor cell phagocytosis in combination with cetuximab. Similar approaches were clinically examined, for example, the combination of CD47/SIRP1a blockers with tumor targeting antibodies such as rituximab and cetuximab. Overall, data presented here point to a potential benefit of combining BND-22 with both anti-PD1/PDL1 and additional therapies.

The data presented in the current report support clinical testing of BND-22 as a potential cancer therapy of solid tumors as monotherapy and in combination with other therapies. A phase I clinical trial of BND-22 in patients with cancer with advanced solid tumors is currently ongoing.

Present affiliations The present affiliation of Hongjing Qu is: Affini-T therapeutics, MA, Watertown, USA and Dmitri Wiederschain is: Jounce Therapeutics, MA, Cambridge, USA.

Acknowledgements We thank everyone that has contributed to the generation and characterization of BND-22. We thank Dr Ohad Ronen and the Galilee Medical Center and Dr Ronit Almog, Dr Sivan Cohen Matsliah and the Rambam Medical Center Biobank, which provided primary tumors and blood samples for this study. We would particularly like to thank the patients that consented to provide the samples. We thank Dr Donald Shaffer, Sanofi for critically reviewing the manuscript.

Contributors DHZ, IG, TP, DA, AFD, MH, RG and HQ designed, preformed, and analyzed in vitro, ex vivo and in vivo mode of action studies. IM, YS, TBM, SS, LP, DW and FON supervised the studies and discussed and interpreted results, SH supervised tissue cross reactivity and toxicology studies. IM and SS wrote the manuscript. YS and IF reviewed the manuscript. TBM is the guarantor.

Funding This study was funded and supported by Biond Biologics and Sanofi.

Competing interests None declared.

Patient consent for publication Not applicable.

Ethics approval This study involves samples obtained from human participants and was approved by Helsinki committee (approval numbers 0626-17-RMB and 0037-18-NHR). The participants gave informed consent to participate in the study before taking part.

Provenance and peer review Not commissioned; externally peer reviewed.

Data availability statement All data relevant to the study are included in the article or uploaded as supplementary information.

ORCID iDs
Ilana Mandel http://orcid.org/0000-0002-4488-5408
Sharad Sharma http://orcid.org/0000-0001-7743-3910

REFERENCES

1 Shiroishi M, Kuroki K, Rasubala L, *et al*. Structural basis for recognition of the nonclassical MHC molecule HLA-G by the leukocyte Ig-like receptor B2 (LILRB2/LIR2/ILT4/CD85d). *Proc Natl Acad Sci U S A* 2006;103:16412–7.
2 Jenkins RW, Barbie DA, Flaherty KT. Mechanisms of resistance to immune checkpoint inhibitors. *Br J Cancer* 2018;118:9–16.
3 Engblom C, Pfirschke C, Pittet MJ. The role of myeloid cells in cancer therapies. *Nat Rev Cancer* 2016;16:447–62.
4 Demaria O, Cornen S, Daëron M, *et al*. Harnessing innate immunity in cancer therapy. *Nature* 2019;574:45–56.
5 Kang X, Kim J, Deng M, *et al*. Inhibitory leukocyte immunoglobulin-like receptors: immune checkpoint proteins and tumor sustaining factors. *Cell Cycle* 2016;15:25–40.
6 Samaridis J, Colonna M. Cloning of novel immunoglobulin superfamily receptors expressed on human myeloid and lymphoid cells: structural evidence for new stimulatory and inhibitory pathways. *Eur J Immunol* 1997;27:660–5.
7 Colonna M, Navarro F, Bellón T, *et al*. A common inhibitory receptor for major histocompatibility complex class I molecules on human lymphoid and myelomonocytic cells. *J Exp Med* 1997;186:1809–18.
8 Wagtmann N, Rojo S, Eichler E, *et al*. A new human gene complex encoding the killer cell inhibitory receptors and related monocyte/macrophage receptors. *Curr Biol* 1997;7:615–8.
9 Kirwan SE, Burshtyn DN. Killer cell Ig-like receptor-dependent signaling by Ig-like transcript 2 (ILT2/CD85j/LILRB1/LIR-1). *J Immunol* 2005;175:5006–15.
10 Shiroishi M, Tsumoto K, Amano K, *et al*. Human inhibitory receptors Ig-like transcript 2 (ILT2) and ILT4 compete with CD8 for MHC class I binding and bind preferentially to HLA-G. *Proc Natl Acad Sci U S A* 2003;100:8856–61.
11 Kim A, Han C-J, Driver I, *et al*. LILRB1 Blockade Enhances Bispecific T Cell Engager Antibody-Induced Tumor Cell Killing by Effector $CD8^+$ T Cells. *J Immunol* 2019;203:1076–87.
12 Dumont C, Jacquier A, Verine J, *et al*. $CD8^+PD^{-1}ILT2^+$ T Cells Are an Intratumoral Cytotoxic Population Selectively Inhibited by the $Immune^-$Checkpoint HLA^-G. *Cancer Immunol Res* 2019;7:1619–32.
13 Cai M-B, Han H-Q, Bei J-X, *et al*. Expression of human leukocyte antigen G is associated with prognosis in nasopharyngeal carcinoma. *Int J Biol Sci* 2012;8:891–900.
14 Carosella ED, Ploussard G, LeMaoult J, *et al*. A systematic review of immunotherapy in urologic cancer: evolving roles for targeting of CTLA-4, PD-1/PD-L1, and HLA-G. *Eur Urol* 2015;68:267–79.
15 Carosella ED, Rouas-Freiss N, Tronik-Le Roux D, *et al*. HLA-G: an immune checkpoint molecule. *Adv Immunol* 2015;127:33–144.
16 Lin A, Yan W-H. Heterogeneity of HLA-G expression in cancers: facing the challenges. *Front Immunol* 2018;9:2164–64.
17 Agaugué S, Carosella ED, Rouas-Freiss N. Role of HLA-G in tumor escape through expansion of myeloid-derived suppressor cells and cytokinic balance in favor of Th2 versus Th1/Th17. *Blood* 2011;117:7021–31.
18 Barkal AA, Weiskopf K, Kao KS, *et al*. Engagement of MHC class I by the inhibitory receptor LILRB1 suppresses macrophages and is a target of cancer immunotherapy. *Nat Immunol* 2018;19:76–84.
19 Lee C-L, Guo Y, So K-H, *et al*. Soluble human leukocyte antigen G5 polarizes differentiation of macrophages toward a decidual macrophage-like phenotype. *Hum Reprod* 2015;30:2263–74.
20 Morandi F, Ferretti E, Castriconi R, *et al*. Soluble HLA-G dampens CD94/NKG2A expression and function and differentially modulates chemotaxis and cytokine and chemokine secretion in CD56bright and CD56dim NK cells. *Blood* 2011;118:5840–50.
21 Dietrich J, Cella M, Colonna M. Ig-like transcript 2 (ILT2)/leukocyte Ig-like receptor 1 (LIR1) inhibits TCR signaling and actin cytoskeleton reorganization. *J Immunol* 2001;166:2514–21.
22 Saverino D, Fabbi M, Ghiotto F, *et al*. The CD85/LIR-1/ILT2 inhibitory receptor is expressed by all human T lymphocytes and down-regulates their functions. *J Immunol* 2000;165:3742–55.

23 Merlo A, Saverino D, Tenca C, *et al*. CD85/LIR-1/ILT2 and CD152 (cytotoxic T lymphocyte antigen 4) inhibitory molecules down-regulate the cytolytic activity of human CD4+ T-cell clones specific for Mycobacterium tuberculosis. *Infect Immun* 2001;69:6022–9.
24 Ince MN, Harnisch B, Xu Z, *et al*. Increased expression of the natural killer cell inhibitory receptor CD85j/ILT2 on antigen-specific effector CD8 T cells and its impact on CD8 T-cell function. *Immunology* 2004;112:531–42.
25 Saverino D, Merlo A, Bruno S, *et al*. Dual effect of CD85/leukocyte Ig-like receptor-1/Ig-like transcript 2 and CD152 (CTLA-4) on cytokine production by antigen-stimulated human T cells. *J Immunol* 2002;168:207–15.
26 Cosman D, Fanger N, Borges L, *et al*. A novel immunoglobulin superfamily receptor for cellular and viral MHC class I molecules. *Immunity* 1997;7:273–82.
27 Navarro F, Llano M, Bellón T, *et al*. The ILT2(LIR1) and CD94/NKG2A NK cell receptors respectively recognize HLA-G1 and HLA-E molecules co-expressed on target cells. *Eur J Immunol* 1999;29:277–83.
28 Morel E, Bellón T. HLA class I molecules regulate IFN-gamma production induced in NK cells by target cells, viral products, or immature dendritic cells through the inhibitory receptor ILT2/CD85j. *J Immunol* 2008;181:2368–81.
29 Leitner J, Kuschei W, Grabmeier-Pfistershammer K, *et al*. T cell stimulator cells, an efficient and versatile cellular system to assess the role of costimulatory ligands in the activation of human T cells. *J Immunol Methods* 2010;362:131–41.
30 Wang Q, Song H, Cheng H, *et al*. Structures of the four Ig-like domain LILRB2 and the four-domain LILRB1 and HLA-G1 complex. *Cell Mol Immunol* 2020;17:966–75.
31 Chapman TL, Heikema AP, West AP, *et al*. Crystal structure and ligand binding properties of the D1D2 region of the inhibitory receptor LIR-1 (ILT2). *Immunity* 2000;13:727–36.
32 Kuroki K, Matsubara H, Kanda R, *et al*. Structural and functional basis for LILRB immune checkpoint receptor recognition of HLA-G isoforms. *J Immunol* 2019;203:3386–94.
33 Zhang Y, Zheng L, Zhang L, *et al*. Deep single-cell RNA sequencing data of individual T cells from treatment-naïve colorectal cancer patients. *Sci Data* 2019;6:131.
34 Gül N, van Egmond M. Antibody-Dependent phagocytosis of tumor cells by macrophages: a potent effector mechanism of monoclonal antibody therapy of cancer. *Cancer Res* 2015;75:5008–13.
35 Siu LL, Wang D, Hilton J, *et al*. First-in-Class Anti-immunoglobulin-like transcript 4 myeloid-specific antibody MK-4830 abrogates a PD-1 resistance mechanism in patients with advanced solid tumors. *Clin Cancer Res* 2022;28:57–70.
36 Carosella ED, Gregori S, Tronik-Le Roux D. HLA-G/LILRBs: a cancer immunotherapy challenge. *Trends Cancer* 2021;7:389–92.
37 Mahoney KM, Rennert PD, Freeman GJ. Combination cancer immunotherapy and new immunomodulatory targets. *Nat Rev Drug Discov* 2015;14:561–84.
38 Choueiri TK, Fishman MN, Escudier B, *et al*. Immunomodulatory activity of nivolumab in metastatic renal cell carcinoma. *Clin Cancer Res* 2016;22:5461–71.
39 Kunert A, Basak EA, Hurkmans DP, *et al*. CD45RA^{+}CCR7^{-} CD8 T cells lacking co^{-}stimulatory receptors demonstrate enhanced frequency in peripheral blood of NSCLC patients responding to nivolumab. *J Immunother Cancer* 2019;7:149.
40 Rebmann* V, Eberhardt* WE, Rizvi N, *et al*. Abstract CT126: soluble HLA-G and -E (sHLA-G/E) as potential biomarkers of clinical outcomes in patients (PTS) with advanced, refractory squamous (SQ) NSCLC treated with nivolumab (NIVO): CheckMate 063. *Cancer Res* 2017;77:CT126–CT26.
41 Mamessier E, Sylvain A, Thibult M-L, *et al*. Human breast cancer cells enhance self tolerance by promoting evasion from NK cell antitumor immunity. *J Clin Invest* 2011;121:3609–22.
42 Roberti MP, Juliá EP, Rocca YS, *et al*. Overexpression of CD85j in TNBC patients inhibits Cetuximab-mediated NK-cell ADCC but can be restored with CD85j functional blockade. *Eur J Immunol* 2015;45:1560–9.
43 Fisher GA, Lakhani NJ, Eng C, *et al*. A phase Ib/II study of the anti-CD47 antibody magrolimab with cetuximab in solid tumor and colorectal cancer patients. *Journal of Clinical Oncology* 2020;38:114–14.
44 Goldman-Wohl DS, Ariel I, Greenfield C, *et al*. HLA-G expression in extravillous trophoblasts is an intrinsic property of cell differentiation: a lesson learned from ectopic pregnancies. *Mol Hum Reprod* 2000;6:535–40.
45 Bluestone JA. Is CTLA-4 a master switch for peripheral T cell tolerance? *J Immunol* 1997;158:1989–93.
46 Godal R, Bachanova V, Gleason M, *et al*. Natural killer cell killing of acute myelogenous leukemia and acute lymphoblastic leukemia blasts by killer cell immunoglobulin-like receptor-negative natural killer cells after NKG2A and LIR-1 blockade. *Biol Blood Marrow Transplant* 2010;16:612–21.
47 Riaz N, Havel JJ, Makarov V, *et al*. Tumor and microenvironment evolution during immunotherapy with nivolumab. *Cell* 2017;171:934–49.

BND-22, A First-in-Class Humanized ILT2-blocking Antibody, Promotes Anti-tumor Immunity and Tumor Regression

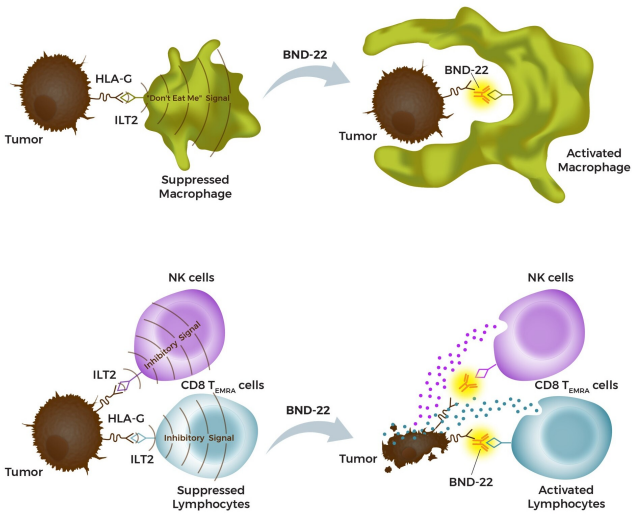

Authors

Ilana Mandel, Dana Haves Ziv, Ilana Goldshtein, Tsuri Peretz, Dror Alishekevitz, Anna Fridman Dror, Motti Hakim, Sharon Hashmueli, Itay Friedman, Yair Sapir, Rita Greco, Hongjing Qu, Frank Nestle, Dmitri Wiederschain, Lily Pao, Sharad K. Sharma, Tehila Ben Moshe

Correspondence

Ilana@biondbio.com

sharad.sharma@sanofi.com

In Brief

BND-22 enhances the activity of innate and adaptive immune cells against tumor cells. BND-22 inhibits ILT2-HLA-G interactions, thus leading to enhanced phagocytosis by macrophages and increased cytotoxic activity of NK cells and CD8 T_{EMRA} T cells against tumor cells.

SUPPLEMENTAL MATERIAL

MATERIALS AND METHODS

Generation of BND-22

BND-22 was generated by immunizing CD1 mice with human ILT2 (ILT2-Fc and ILT2-HIS; Sino Biological, 16014-H02H, R&D systems, 8989-T2) using hybridoma technology (Precision Antibody). The antibody that demonstrated superior binding and activity was humanized using Germ-Line Humanization (CDR-grafting) technology (Antitope Ltd.). Humanized V region genes were designed based upon human germline sequences with the closest homology to a chimeric version of the antibody and made using gene synthesis. These were then cloned into vectors containing IgG4 (S241P, L235E) heavy chain genes together with human kappa light chain genes. The antibodies and all combinations of CDR-grafted heavy and light chains were expressed in HEK293-EBNA cells. The clone with optimal binding to human and cynomolgus monkey ILT2, blocking and functional activity was chosen for further development as BND-22.

FACS analysis of ILT2 Expression in immune cell subsets

Approximately $5x10^5$ cells per sample were incubated with a commercial ILT2 antibody or PE-conjugated BND-22 in FACS staining buffer (10% human serum in PBS) for 30 minutes. In order to identify different immune cell populations, the following markers were used: CD45, CD4, CD8, CD14, CD11b, HLA-DR, CD33, CD56, CCR7, CD45RA or the appropriate isotype controls (all antibodies from Biolegend). Cell viability was determined with Fixable Viability stain 780 (BD biosciences) and the

cells were analyzed using the Cytoflex flow cytometer (Beckman Coulter). The data were analyzed using CytExpert software (Ver 2.3). The various immune cell populations were defined as detailed in the following table

Immune cells subpopulation	**PBMC**	**Fresh tumors**
Total immune cells	Live CD45+	Live CD45+
CD8 T cells	Live CD45+ CD4-CD8+	Live CD45+ CD4-CD8+
CD4 T cells	Live CD45+CD8-CD4+	Live CD45+CD8-CD4+
T_{EMRA} CD8 T cells	NA	Live CD45+CD8+CD4-CCR7-CD45RA+
NK cells	Live CD45+CD8-CD56+	Live CD45+CD8-CD56+
Monocytes	Live CD45+CD14+ CD11b+	NA
TAM	NA	Live CD45+ CD33+ CD14+HLA-DR+

Bioinformatic analysis

Normalized enrichment score (NES) values for different immune cell types were downloaded from the TCIA database for all TCGA patients. These data where then combined with the individual ILT2 gene expression values for each patient of interest from the TCGA to create a data set that analyze individual cell type enrichment stratified by gene-level expression. In a separate analysis, TCGA RNAseq expression data was analyzed across multiple cancer types. CD8-expressing samples were defined as those with expression above the quartile. The percentage of patients with high T_{EMRA} levels were identified based on high expression (above median) of the T_{EMRA} signature genes KLRG1 and CX3CR1, out of the CD8-expressing samples. In addition, the RNAseq data published by Riaz et al., 2017, Cell, was used to calculate change in expression s of ILT2 in melanoma patients treated with anti-PD-1. An additional analysis was preformed to evaluate ILT2 and PD-1 expression in intra-tumoral CD8 T cells from CRC patients documented in http://crctcell.cancer-pku.cn/.

Binding of BND-22 Human ILT2

Kinetic experiments were performed by Biacore T200 (GE Healthcare) and Evaluation softwareV3.0 (GE Healthcare) in order to evaluate the binding kinetics and affinity between BND-22 to human ILT2 (ILT-His – Novus, 8989T2050; Sino biologics, 16014-H08H; LS-Bio, LS-G97658). A multi-cycle kinetics analysis was preformed using a Protein A capture Sensor chip. A running buffer of HBS-P+ (pH 7.4)

was used and a two-fold dilution range was selected from 25.0 nM to 0.78 nM of ILT2. A 1:1 Langmuir binding analysis was used to analyze the results.

In order to evaluate the binding of BND-22 to membranal ILT2, approximately $5x10^5$ BW-ILT2 cells were incubated with BND-22 conjugated to PE (Biosciences, 703-0005) or with a PE-conjugated isotype control (Biolegend, 400113) in staining buffer (0.05% BSA in PBS) for 30 minutes. Cells were then washed twice using staining buffer and analyzed using the Cytoflex flow cytometer (Beckman Coulter). The data were analyzed using CytExpert software (Ver 2.3).

Binding of BND-22 to other ILT family members

Maxisorp 96 well plates were coated overnight with ILT6-His (Sino Biological,13549-H08H), ILT4-FC (Sino Biological, 4132-H02H) LILRA1-His (Sino Biological, 17220-H08H) in CBC buffer (KPL; cat No C3041) followed by blocking for 1 hour in 1% Casein (Thermo, 37528). BND-22 or positive control ILT4, LILRA1, ILT6 antibodies (Biolegend, 42D1, 338704; R&D systems, MAB3085; Sino Biological, 13549-MM06, respectively) were then added to the plates. A secondary peroxidase-conjugated goat anti human kappa chain (Sigma Aldrich, A7164) or anti-rat antibody (Jakcson, 712-035-153) were added to the plates after washing, followed by detection using TMB. The absorbance was measured using an ELISA Reader (Biotek Synergy-H1 plate reader).

Approximately $5x10^5$ BW-ILT4 cells were incubated with BND-22 conjugated to PE (Innova Biosciences, 703-0005) or with a PE-conjugated isotype control (Biolegend, 400113) in staining buffer (0.05% BSA in PBS) for 30 minutes. Cells were then washed twice using staining buffer and analyzed using the Cytoflex flow cytometer (Beckman Coulter). The data were analyzed using CytExpert software (Ver 2.3). As a positive control for binding to ILT4, an ILT4-binding antibody was included in the assay (Biolegend, 42D1, 338704).

Blocking activity of BND-22

A375-HLA-G were incubated with biotinylated ILT2-FC (Sino Biologics, 1614-H02H; Innova Biosciences, 370-0010) in the presence of BND-22. The binding of ILT2-biotin to the cells was determined using Streptavidin-PE by flow cytometry analysis.

BW cells stably transfected with a chimeric molecule composed of the extracellular portion of human ILT2 fused to mouse z-chain (BW/ILT2-Zeta) were incubated A375-HLA-G or various 721.221 cells in the presence of the BND-22 or a control IgG4 (Biolegend, 403702) or no antibody (medium). The secretion of a mouse IL2 was determined after 48 hours of incubation by ELISA (Biolegend, 431003).

Phagocytosis assays

Monocytes were isolated from buffy coat samples obtained from healthy blood bank donors using a human monocyte enrichment kit (Stem Cells, 15068). The monocytes were grown in RPMI medium supplemented with 10% human serum and M-CSF (50 ng/ml; R&D systems, 216-MC) for 6-7 days in order to generate macrophages. The ability of macrophages to phagocyte tumor cells was examined using a real-time IncuCyte analysis system. Target cell lines were labeled with pHrodo Red Cell Labeling Dye (Satorius, 4649), washed and added to macrophages along with various treatments in replicates (IgG4, Biolegend 403702; BND-22; Erbitux, Merck KGaA; anti-CD47, B6H12). The fluorescence of the pHrodo Red Cell Labeling Dye is increased in an acidic environment such as the one that is resident in the phagosome, thus enabling the quantitation of phagocytosis events by measurement of fluorescence. The IncuCyte instrument (IncuCyte S3 live-cell imaging system; Satorius) sampled the assay plate every 30min for fluorescent red signal intensity and phase images. Phagocytosis events are reflected as accumulation of red fluorescent signal. A threshold of red signal was established for each experiment according to the signal of the tumor cells only wells. The background levels of the tumor cells only were subtracted from the MFI calculated for the different treatments. In order to calculate the present increase from control IgG the following equation was used: 100×(sample-control IgG)/(control IgG)

T cell activity assays

Jurkat wild-type or Jurkat transfected to express human ILT2 (Jurkat-ILT2) (50,000 cells) were co-cultured with mitomycin-treated (30µg/ml) A375 wild-type cells transfected with OKT3scFv-CD14 (A375-WT-OKT3) or A375-HLA-G cells transfected with OKT3 scFv-CD14 (A375-HLA-G-OKT3) (10,000 cells) in the presence of different concentrations of BND-22, an HLA-G-specific antibody (G-0031) or a control hIgG4 (Sino Biologics, HG4K). The amount of secreted human IL2 was evaluated by a commercial ELISA kit following 48 hours.

For MLR assays, dendritic cells generated from monocytes and CD8 T cells (T cells) were isolated from different healthy human donors. The cells were combined in an E:T of 5:1 together with the indicated treatments followed by detection of IFNγ secretion on day 5 by MSD.

For signaling assays, TIL ($120x10^3$ / well) were co-cultured with A375-HLA-G-OKT3 cells in an E:T ratio of 2:1 for 2, 5 and 15 minutes in the presence or absence of BND-22 (20 µg/ml). At each time point, the cells were fixed using 2% PFA (EMS, 15710) followed by permeabilization (Bactlab Diagnostics, 554723). The levels of phosphorylated ZAP70 were evaluated by flow cytometry using antibodies for

CD57, CD28, ILT2 and phospho-ZAP70 (Biolegend 322316, 302906; eBioscience 17-5129-42, 12-9006-41, respectively) or the appropriate isotype controls. Cells were evaluated using the Cytoflex flow cytometer and analyzed using CytExpert software (Ver 2.3).

For ex vivo experiments, single cell tumor suspensions ($0.5X10^5$) were co-cultured with autologous PBMC ($0.5X10^6$) in the presence of IL-2 (50 U/ml; Proleukin Novartis Pharma) and the indicated antibodies (BND-22, human IgG4 Biolegend,403702) and/or anti-PD-1 (Pembrolizumab, Merck MSD) for 5-6 days after which the secretion of TNFa was evaluated by ELISA (Invitrogen, 88-7346-86).

NK cell activity assays

Killing assays were conducted by co-culturing NK cells with different target cell lines including A375 and A253 cells, with or without transfection of HLA-G in the presence of different concentrations of BND-22. Effector NK cells (1.5x105) were pre-incubated for 30 minutes with increasing concentrations of BND-22. Target MHC-I or HLA-G positive target cells at an E:T of 7.5:1 were added and incubated for 5 additional hours at 37°C. IgG4 (Sino Biologics, HG4K) was used as a negative control. Cytotoxicity levels were determined using a fluorometric Lactate dehydrogenase (LDH) detection kit (CytoTox ONE Homogeneous, Promega, G7890) according to the manufacturer's instructions. Fluorescence was measured using an ELISA Reader (Biotek Synergy-H1 plate reader). Percent of specific cytotoxicity was calculated as

$$\% \text{ Cytotoxicity} = \frac{100\ x\ (Test\ sample - Low\ control\ (target\ cells\ only))}{(High\ control\ (target\ cells\ in\ lysis\ buffer) - Low\ control - effectors\ only)}$$

The supernatants were used in parallel for quantification of Granzyme B and IFNγ secretion (Granzyme B – 5 hours; IFNγ – 24 hours) with commercial ELISA kits according to the manufacturers' instructions (Mabtech, 3485-1H-20; Biolegend, 430101, respectively).

Primary NK cells were isolated from buffy coat samples obtained from healthy blood bank donors using a human NK enrichment kit (Stem Cells, 15065). The NK cells were grown in complete RPMI medium supplemented with IL2 (50 IU/ml) for 2 days. On the day of the experiment, the NK cells ($1.5x10^5$/well) were incubated with target cancer cell lines at E:T ratio of 8:1 in the presence BND-22 or control human IgG together with Golgi stop. for 5 hours at 37°C. The levels of intracellular IFNγ and membranal CD107a were evaluated by flow cytometry. Briefly, the cells were stained with the appropriate antibodies for membranal targets including CD3, CD56, CD107a, ILT2 (Biolegend, 317306, 362510, 32862; eBioscience, 17-5129-4, respectively). The cells were than fixed and permeabilized using an appropriate kit (Fixation/Permeabilization kit, Bactlab Diagnostics, 554715) followed by staining of intracellular IFNγ (Biolegend, 506507). Appropriate isotype controls were

used as controls. Viability of the cells was assessed with a viability dye (Bactlab Diagnostics, 565388) followed by analysis with the Cytoflex flow cytometer (Beckman Coulter).

For signaling experiments, NK cells ($120x10^3$ / well) were co-cultured with A253-HLA-G cells in an E:T ratio of 4:1 for 1-15 minutes in the presence or absence of BND-22 (50 µg/ml). At each time point, the cells were fixed by 4% PFA (EMS, 15710) on ice followed by permeabilization (Bactlab Diagnostics, 554723). The levels of phosphorylated ZAP70/Syk was evaluated by flow cytometry using appropriate antibodies including CD56, ILT2 and phspho- ZAP70/Syk (Biolegend 362510; eBioscience, 17-5129-42, 12-9006-41, respectively) , isotype controls and analyzed using the Cytoflex flow cytometer (Beckman Coulter).

FACS analysis of tumor samples from lung lesion metastasis model

Fresh lung samples obtained from the mice were digested into single cell suspensions using an enzymatic mixture of DNase 1 type IV (30U/ml), Hyaluronidase type V (100 µg/ml) and Collagenase (1 mg/ml). Approximately $1x10^6$ cells per sample were incubated with a commercial ILT2 antibody and different antibody mixes (10% human serum in PBS) for 30 minutes. The following markers were used: CD45, CD4, CD8, CD25, CD56, CD69, CD45RA, CD197(CCR7), CD107a, (Biolegend, 368522, 200103, 301006, 302216, 362504, 310912, 304106, 353212, 328626, 329908 respectively) or the appropriate isotype controls. Cell viability was determined with Fixable Viability stain 780. Cells were then washed twice using staining buffer and analyzed using the Cytoflex flow cytometer (Beckman Coulter).

FACS analysis of tumor samples from humanized mice model

At termination, tumors were digested into single cell suspensions and evaluated by FACS analysis for the following markers: 7AAD, hCD45, hCD11b, HLA-DR, ILT2, hCD68, hCD80, hCD206, hCD83, PD-1, hCD45RA, hCCR7, hCD14, hCD56, hCD4 and hCD8.The gating strategy depicted in the following table was used to define the different immune cell populations.

Immune cells subpopulation	**Gating strategy**
Total immune cells	Live CD45+
TAM	Live CD45+CD33+HLA-DR+CD14+
M1 (pro-inflammatory macrophages)	Live CD45+CD33+HLA-DR+CD14+CD80+
M2 (anti-inflammatory macrophages)	Live CD45+CD33+HLA-DR+CD14+CD80-CD83-
DC	Live CD45+CD33+HLA-DR+CD14-
CD8 T cells	Live CD45+ CD3+CD4-CD8+
NK cells	Live CD45+CD3-CD56+

Figure S1

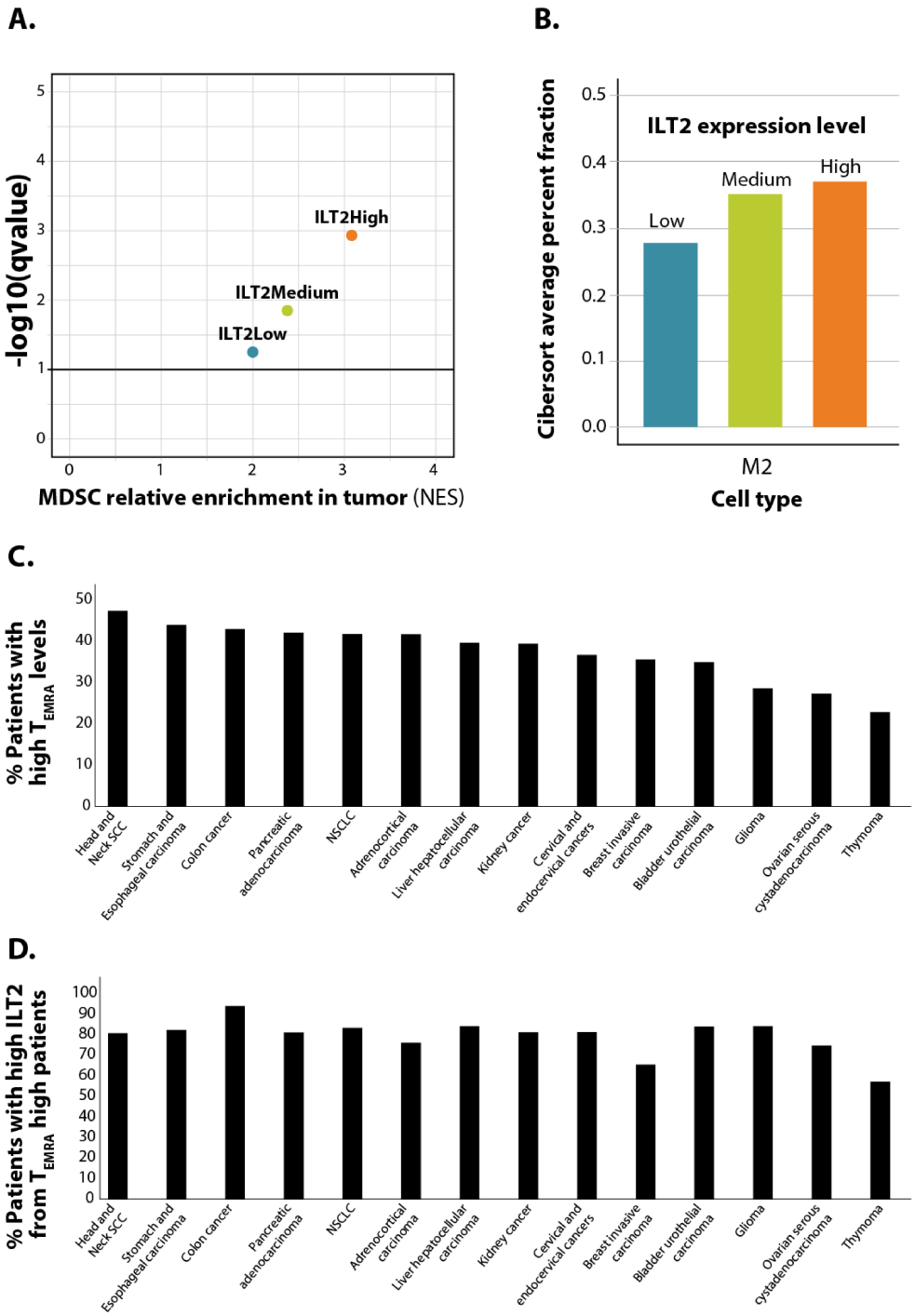

Figure S1: ILT2 expression in the TME is correlated with enrichment of MDSC, M2 and T_{EMRA} CD8 T cells in different cancer indications

(**A**) Normalized enrichment score (NES) values for all MDSC were downloaded from the TCIA database for all TCGA patients. These data where then combined with the individual gene expression values for each patient of interest to create a data set to analyze individual cell type enrichment stratified by gene-level expression. A plot of MDSC enrichment in patients with low, medium and high ILT2 levels is presented. (**B**) Cibersort was used to analyze cell fractionation for M2 cell types analyzed across patients expressing low, medium and high ILT2 levels. An analysis of patients that contained above 25% quartile levels of CD8 was performed for each indication present in the TCGA. (**C**) The levels of TEMRA-specific genes (KLRG1+CX3CR1+) was determined. The graph presents the percent of patients for each indicated cancer type that had high T_{EMRA} levels (above median). (**D**) The percent of patients from the patients presented in **C**. which had high ILT2 levels (above median) is shown.

Figure S2

A.

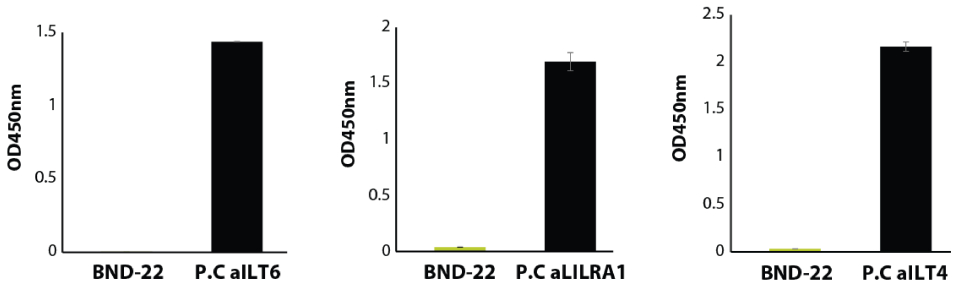

B.

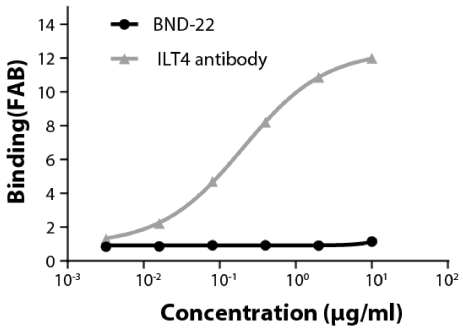

Figure S2: BND-22 shows no binding to ILT6, LILRA1 and ILT4

(**A**) The binding of BND-22 to human ILT6, LILRA1 and ILT4 was determined by an ELISA-based assay in comparison to positive control antibodies which bind these proteins. The absorbance at 450nm with 650nm as a reference is presented. (**B**) The binding to BW-ILT4 cells was evaluated using a PE-labeled BND-22 antibody and analyzed by flow cytometry in comparison to a positive control anti ILT4 antibody. FAB (fold above background) levels of BND-22 or anti ILT4 binding compared to the isotype control at the different concentrations examined were plotted using a 4-parameter analysis. P.C – positive control. P.C ILT6 – anti-ILT6 Ab, P.C LILRA1 – anti-LILRA1 Ab, P.C – anti-ILT4 Ab.

Figure S3

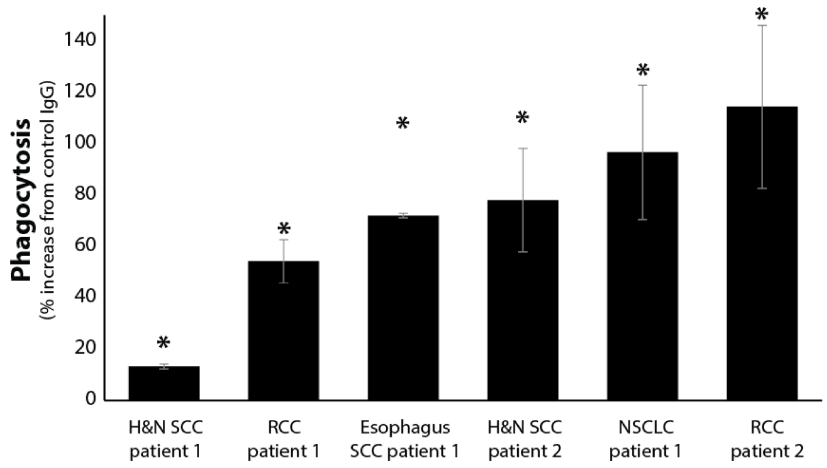

Figure S3: BND-22 enhances the phagocytosis of tumor cells from cancer patients by macrophages

Single cell suspensions were generated by enzymatic digestion of fresh tumors isolated from operations of the indicated patients. The cells were stained with pHrodo Red Cell Labeling Dye, washed and mixed with macrophages generated from monocytes isolated from healthy donors along with BND-22 or control IgG. The percent of phagocytosis increase compared to macrophages and target cells with control IgG at a singular time point is presented. *P<0.05; un-paired Student's T-test compared to cells with control IgG.

Figure S4

A.

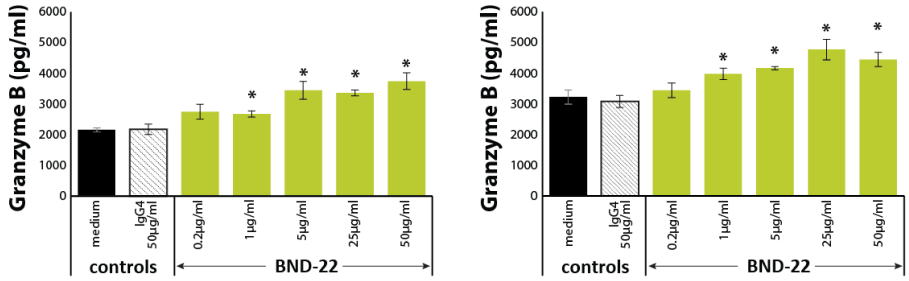

B.

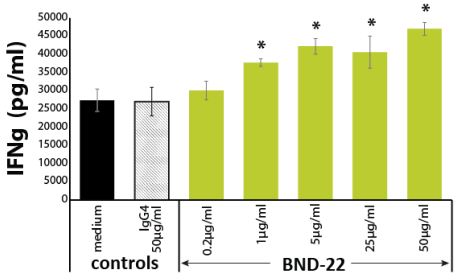

Figure S4: BND-22 enhances Granzyme B and IFNγ secretion of NK cells in the presence of cancer cell lines

NK cells were incubated with the indicated concentrations of BND-22 (batch BND-22-T) or an isotype matched control IgG; Target cells including A375-HLA-G (**A**), A253-WT (**B**) and A253-HLA-G (**C**) were added for additional 5 hours at effector-to-target ratio of 7.5:1. Granzyme B and IFNγ secretion were measured by ELISA. Results represent the mean + S.E of values from 3 repeats per treatment.

Figure S5

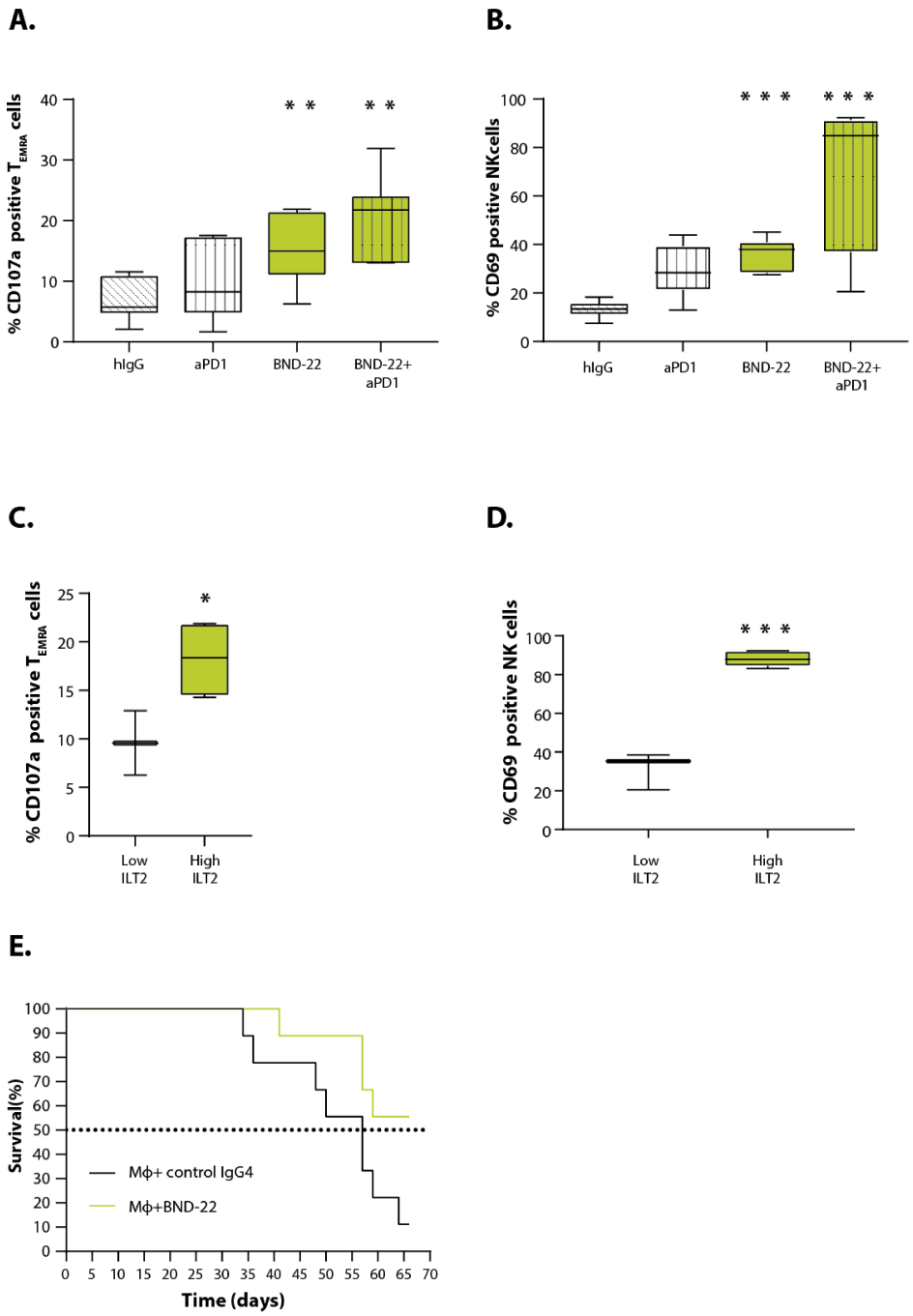
A.
% CD107a positive T_{EMRA} cells
40
30
20
10
0
* *
* *
hIgG
aPD1
BND-22
BND-22+ aPD1
B.
% CD69 positive NKcells
100
80
60
40
20
0
* * *
* * *
hIgG
aPD1
BND-22
BND-22+ aPD1
C.
% CD107a positive T_{EMRA} cells
25
20
15
10
5
0
*
Low ILT2
High ILT2
D.
% CD69 positive NK cells
100
80
60
40
20
0
* * *
Low ILT2
High ILT2
E.
Survival(%)
100
90
80
70
60
50
40
30
20
10
0
Mϕ+ control IgG4
Mϕ+BND-22
0 5 10 15 20 25 30 35 40 45 50 55 60 65 70
Time (days)

F.

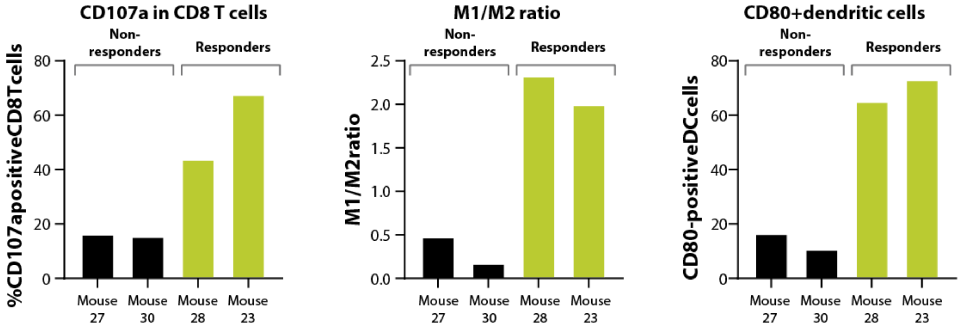

G.

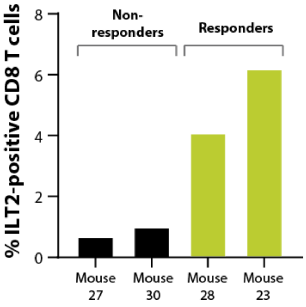

Figure S5: The anti-tumor in vivo activity of BND-22 is mediated by the activation of different immune cells in correlation with ILT2 expression

SCID-NOD mice were engrafted by IV administration with MEL526-HLA-G cells. Human PBMC isolated from healthy donors were administrated to the relevant groups together with IL-2 and the relevant treatments (10 mg/kg each) starting from day 14 (**A-D**). The levels of CD107a in T_{EMRA} T cells (**A**) and CD69 in NK cells (**B**) in the lungs of the treated mice. CD107a (**C**) and CD69 (**D**) expression in BND-22 treated T_{EMRA} or NK cells in mice that received PBMC from donors with low or high levels of ILT2 in their T_{EMRA} cells or NK cells, respectively. The results represent the average of tumor weight ±SE from 5-9 mice per treatment group. Un-paired T test was used to calculate statistical significance between the groups * $P < 0.05$. ** $P < 0.005$. *** $P < 0.0005$. SCID-NOD mice were engrafted SC with COLO-320-HLA-G cells in parallel to injection of macrophages generated from 3 healthy donors. The animals were treated with BND-22 or with a control human IgG4 SC on day 0 followed by 4 additional injections IV. (**E**). Survival analysis was preformed using a Kaplan-Meier curve. Log-rank (Mantel-Cox) test was used to was used to calculate statistical significance in survival between the groups * $P < 0.05$. Humanized NSG mice were engrafted with CD34+ immune cells from human donors. After 14 weeks, the mice received subcutaneous injections of A253-HLA-G cancer cells. Once the tumors were established (80mm^3), the mice were administered IV with BND-22 or control hIgG4 twice a week. (**F**). At day 46 the mice were sacrificed, and the levels of different markers were evaluated by FACS analysis. CD107a in CD8 T cells, M1/M2 ratios and the levels of CD80+ dendritic cells in the tumors of the indicated mice are presented. (**G**) Baseline ILT2 levels in peripheral CD8 T cells of the indicated mice.

Table S1: Rate constants for the modified peptides of ILT2 derived from HRF and trypsin digestion

Position in ILT2	Sequence of ILTS SEQ ID NO: ( )	Free ILT2, *K*free, s-1	ILT2-BND-22com, *K*com, s-1	Ratio, *K*free/*K*com	NR Ratio/1.44
5-24	PTLWAEPGSVITQGSPVTLR (22)	8.93 ± 1.86	7.04 ± 1.24	1.27	0.88
25-35	CQGGQETQEYR (23)	1.18 ± 0.11	0.77 ± 0.070	1.53	1.06
42-48	TALWITR (24)	2.62 ± 0.50	1.56 ± 0.26	1.68	1.17
49-55	IPQELVK (25)	2.41 ± 0.42	1.5 ± 0.24	1.61	1.12
56-71	KGQFPIPSITWEHAGR (3)	9.09 ± 0.87	2.31 ± 0.17	3.94	**2.74**
57-71	GQFPIPSITWEHAGR (4)	6.93 ± 0.68	1.97 ± 0.38	3.52	**2.44**
74-83	CYYGSDTAGR (26)	0.58 ± 0.057	0.32 ± 0.078	1.81	1.26
84-100	SESSDPLELVVTGAYIK (5)	1.26 ± 0.15	0.37 ± 0.055	3.41	**2.35**
101-134	PTLSAQPSPVVNSGGNVILQCDSQVAF DGFSLCK (27)	5.46 ± 0.85	11.08 ± 1.94	0.49	0.34
135-151	EGEDEHPQCLNSQPHAR (28)	5.62 ± 0.81	6.81 ± 1.08	0.83	0.58
156-167	AIFSVGPVSPSR (29)	1.51 ± 0.20	1.0 ± 0.13	1.51	1.05
156-168	AIFSVGPVSPSRR (30)	1.6 ± 0.17	0.94 ± 0.013	1.7	1.18
168-172	RWWYR (31)	0	0	-	-
173-200	CYAYDSNSPYEWSLPSDLLELLVLGVSK (32)	7.67 ± 0.73	5.39 ± 0.57	1.42	0.99
201-230	KPSLSVQPGPIVAPEETLTLQCGSDAGY NR (33)	4.24 ± 0.37	2.64 ± 0.19	1.61	1.12
236-265	DGERDFLQLAGAQPQAGLSQAN*FTLG PVSR (34)	4.55 ± 0.84	3.21 ± 0.40	1.41	0.98
240-265	DFLQLAGAQPQAGLSQAN*FTLGPVSR (35)	3.55 ± 0.70	2.37 ± 0.11	1.5	1.04
240-265	DFLQLAGAQPQAGLSQ ANFTLGPVSR (36)	1.96 ± 0.24	1.55 ± 0.17	1.26	0.88

266-272	SYGGQYR (37)	0	0		-
273-301	CYGAHNLSSEWSAPSDPLDILIAGQFYD R (38)	5.83 ± 0.83	5.16 ± 0.82	1.13	0.78
336-344	EGAADDPWR (39)	5.37 ± 0.69	5.33 ± 0.98	1	0.69
354-372	YQAEFPMGPVTSAHAGTYR (40)	23.01 ± 6.49	15.19 ± 1.98	1.51	1.05
373-380	CYGSQSSK (41)	0	0	-	-

Table S2: Rate constants for the modified peptides of the ILT2 derived from HRF and trypsin/Asp-N digestion

Position	**Sequence SEQ ID NO: ( )**	**Free ILT2, *K*free, s-1**	**ILT2-BND-22com, *K*com, s-1**	**Ratio, *K*free/*K*com**	**NR Ratio/1.53**
5-24	PTLWAEPGSVITQGSPVTLR (42)	15.07 ± 1.16	19.66 ± 1.7	0.78	0.51
10-24	EPGSVITQGSPVTLR (43)	1.91 ± 0.97	1.05 ± 0.030	1.82	1.19
42-48	TALWITR (44)	2.84 ± 0.49	1.74 ± 0.31	1.63	1.07
49-55	IPQELVK (45)	2.69 ± 0.42	2.02 ± 0.32	1.33	0.85
57-66	GQFPIPSITW (6)	4.32 ± 0.51	0.72 ± 0.082	6	**3.92**
91-100	ELVVTGAYIK (7)	0.70 ± 0.082	0.14 ± 0.0071	5	**3.27**
138-151	EDEHPQCLNSQPHAR (46)	0.82 ± 0.11	0.77 ± 0.14	1.06	0.69
156-167	AIFSVGPVSPSR (47)	1.8 ± 0.21	1.15 ± 0.088	1.57	1.03
183-193	EWSLPS (48)	0.52 ± 0.11	0.33 ± 0.065	1.58	1.03
189-200	DLLELLVLGVSK (49)	2.92 ± 0.27	1.81 ± 0.017	1.61	1.05
192-200	ELLVLGVSK (50)	1.16 ± 0.21	0.84 ± 0.13	1.38	0.9
266-272	SYGGQYR (51)	0	0	-	-
291-299	DILIAGQFY (52)	0.89 ± 0.092	0.44 ± 0.066	2.02	1.32
354-372	YQAEFPMGPVTSAHAGTYR (53)	5.98 ± 0.90	3.35 ± 0.27	1.79	1.17
357-372	EFPMGPVTSAHAGTYR (54)	18.19 ± 2.27	15.01 ± 1.98	1.21	0.79

Epitope mapping was performed using hydroxyl radical foot-printing (HRF) and mass spectrometry techniques. Briefly, the ILT2-BND-22 or only ILT2 were exposed to hydroxyl radicals followed by digestion with Trypsin and AspN and liquid chromatography coupled with high-resolution mass spectrometry (LC-MS). The retrieved MS data comparing the protein and antibody-protein complex were used to map the epitope of the antibody. The rate constants for the modified peptides of ILT2 following trypsin digestion (Table 1S) or trypsin/Asp-N digestion (Table 2S) are presented. The highest normalized protection ratio (NR) values are bolded.